AGU PUBLICATIONS

JGR

Journal of Geophysical Research: Oceans

RESEARCH ARTICLE

10.1002/2017JC013345

Multiphase Reactive Transport and Platelet Ice Accretion in the Sea Ice of McMurdo Sound, Antarctica

J. J. Buffo[1], B. E. Schmidt[1], and C. Huber[1,2]

[1]School of Earth and Atmospheric Sciences, Georgia Institute of Technology, Atlanta, GA, USA, [2]Now at Department of Earth, Environmental and Planetary Sciences, Brown University, Providence, RI, USA

Key Points:
- A one-dimensional finite difference model capable of simulating multiphase reactive transport and platelet ice accretion in growing sea ice
- Model simulates platelet ice accretion due to ice shelf water plumes and demonstrates its effect on nearby sea ice volume and structure
- Creation and validation of a one-dimensional parameterization of platelet ice primed for incorporation into larger systems models

Supporting Information:
- Supporting Information S1

Correspondence to:
J. Buffo,
jacob.buffo@eas.gatech.edu

Citation:
Buffo, J. J., Schmidt, B. E., & Huber, C. (2018). Multiphase reactive transport and platelet ice accretion in the sea ice of McMurdo sound, Antarctica. *Journal of Geophysical Research: Oceans*, *123*. https://doi.org/10.1002/2017JC013345.

Received 8 AUG 2017
Accepted 21 DEC 2017
Accepted article online 28 DEC 2017

Abstract Sea ice seasonally to interannually forms a thermal, chemical, and physical boundary between the atmosphere and hydrosphere over tens of millions of square kilometers of ocean. Its presence affects both local and global climate and ocean dynamics, ice shelf processes, and biological communities. Accurate incorporation of sea ice growth and decay, and its associated thermal and physiochemical processes, is underrepresented in large-scale models due to the complex physics that dictate oceanic ice formation and evolution. Two phenomena complicate sea ice simulation, particularly in the Antarctic: the multiphase physics of reactive transport brought about by the inhomogeneous solidification of seawater, and the buoyancy driven accretion of platelet ice formed by supercooled ice shelf water onto the basal surface of the overlying ice. Here a one-dimensional finite difference model capable of simulating both processes is developed and tested against ice core data. Temperature, salinity, liquid fraction, fluid velocity, total salt content, and ice structure are computed during model runs. The model results agree well with empirical observations and simulations highlight the effect platelet ice accretion has on overall ice thickness and characteristics. Results from sensitivity studies emphasize the need to further constrain sea ice microstructure and the associated physics, particularly permeability-porosity relationships, if a complete model of sea ice evolution is to be obtained. Additionally, implications for terrestrial ice shelves and icy moons in the solar system are discussed.

1. Introduction

Sea ice is a ubiquitous feature of the Earth's polar regions and, as the boundary between the hydrosphere and atmosphere, it plays a critical role in both local and global climatic, oceanic, and biological processes (Thomas, 2017). With north polar sea ice maximums decreasing at unprecedented rates (Thomas, 2017), it is imperative to understand and quantify the physical, thermal, and chemical processes that affect the evolution of sea ice. Sea ice plays an important role in facilitating Arctic and Antarctic water mass formation that in turn affects global ocean circulation (Meredith & Brandon, 2017). It sources high salinity shelf water, crucial in determining basal melt rates and stability of floating ice shelves, slowing mass loss of the Antarctic and Greenland ice sheets (Joughin & Alley, 2011). It provides a refuge for ice algae, a key primary producer in the polar oceans, along with other microfauna and macrofauna in its lower layers (Loose et al., 2011; Vancoppenolle et al., 2013). Understanding how these organisms persist within the ice can help elucidate their survival mechanisms and has potential astrobiological application to putative ice-ocean interfaces elsewhere in the solar system (Greeley et al., 1998; Soderlund et al., 2013; Thomas & Dieckmann, 2009; Wettlaufer, 2009).

Compared to freshwater ice, sea ice is dynamic and complex, due primarily to the inherent impurities of seawater. When a solution, such as seawater, is cooled below its freezing point the solvent (water) begins to solidify while the solute (salt) is preferentially rejected from the crystalline lattice increasing the concentration (salinity) of the remaining liquid fraction (Feltham et al., 2006; Wettlaufer et al., 1997). A similar process dictates the fractional crystallization of magmas and metal alloys (Emms & Fowler, 1994; Worster, 1997; Worster et al., 1990), although in a vastly different temperature regime. In the case of ocean water, the result is a porous crystalline ice matrix flush with brine-filled pockets and channels. The two-phase nature of this system determines the thermal, chemical, and mechanical properties of the ice and allows for fluid and solute transport (Petrich & Eicken, 2017). The physics governing the formation and reactive transport processes affecting sea ice are well summarized by mushy layer theory, which treats ice as a multiphase reactive porous media (Feltham et al., 2006; Hunke et al., 2011).

The fact that there exist impurities within sea ice has been known for nigh on a century (see Malmgren, 1927), and documentation of its heterogeneities, as well as the impact they have on the mechanical and thermal properties of the ice, has been carried out ever since (Cox & Weeks, 1974; Eicken, 1992, 2003; Schwerdtfecer, 1963). Worster and Rees Jones (2015) provide a comprehensive review of the laboratory experiments (i.e., Huppert & Worster, 1985), and theoretical work (Feltham et al., 2006; Huppert & Worster, 1985; Worster, 1991), that has led to contemporary models of sea ice (Griewank & Notz, 2013, 2015; Rees Jones & Worster, 2014; Turner et al., 2013; Vancoppenolle et al., 2007; Wells et al., 2011). While these models have improved drastically over the years, and have greatly increased our understanding of the small-scale physics that dictate the formation and evolution of sea ice, there remain numerically unconstrained processes and others that need refinement (Petrich & Eicken, 2017).

Sea ice near the termini of ice shelves is subject to an additional phenomenon known as platelet ice accretion. Here a buoyant plume of supercooled water (below its in situ freezing point) created by pressure melting at the basal surface of the abutting ice shelf upwells from the ice shelf cavity and bathes the underside of the sea ice. As the plume rises, and the in situ freezing point increases, small ice crystals (platelets) begin to nucleate in the water column to relieve the thermodynamically unstable supercooling. The crystals continue to grow until buoyant forces lead them to rise upward, where they accrete onto the basal surface of the sea ice (Dempsey et al., 2010; Gough et al., 2012; Leonard et al., 2006). These floating crystals modify the ice-ocean interface, creating a highly porous layer of platelet ice with notably different crystal geometry and texture than the typical granular or columnar ice produced by the direct freezing of ocean water onto the sea ice-ocean interface (Dempsey et al., 2010; Dempsey & Langhorne, 2012). The addition of platelet ice crystals to the sea ice layer can modify the thermal and mechanical properties of the ice as well as contribute meters of consolidated platelets to the overall ice thickness (with maximums near ice shelf fronts reaching $\sim$10 m; Eicken & Lange, 1989; Hellmer, 2004; Hoppmann et al., 2015; Hunkeler et al., 2016). Quantifying this interaction between sea ice and ice shelves and incorporating it into numerical simulations of platelet-affected ice would improve the fidelity and predictions of such models, increasing our understanding of polar ice-ocean interactions.

Platelet ice was first recorded in the literature a half century ago (Dayton et al., 1969), and while a number of observations have documented the existence, structure, ecology, and regional abundance of platelet ice (Arrigo et al., 1995; Dempsey et al., 2010; Gough et al., 2012; Jeffries & Weeks, 1993; Leonard et al., 2006; Smith et al., 2001), nearly all numerical models exclude it from their treatment of sea ice—with notable exceptions (Dempsey, 2008; Dempsey et al., 2010; Kawano & Ohashi, 2008; Ohashi et al., 2004; Ohashi & Kawano, 2007). The most extensive and complete model of platelet ice accretion to date is the work of Wongpan et al. (2015), wherein the authors simulate platelet ice rise dynamics as well as diffusive heat and salt transport within the subice platelet layer. The result is an extremely high fidelity three-dimensional simulation of a small portion (10 cm $\times$ 10 cm $\times$ 10 cm) of the advancing sea ice-ocean interface. The model excludes fluid dynamics such as advection and convection but does artificially increase the thermal and chemical diffusion constants in an attempt to remedy this. Different model techniques have their own benefits and limitations. Purely mechanical models can simulate larger domains but cannot accurately recreate the thermal and chemical physics occurring in the forming layer. These physics are partially captured in the models of Kawano and Ohashi (2008) and Wongpan et al. (2015) but the computational expense of these models limits them to much smaller spatial scales.

Formation of ice crystals in a supercooled water column also occurs beneath ice shelves and in rivers (see Martin, 1981). Daly (1984) provides a comprehensive background on the subject, covering the formation, evolution, dynamics, and size distribution of frazil ice. Modeling efforts have sought to simulate the physical and thermal evolution of these ice-laden waters (Jenkins & Bombosch, 1995; Holland & Feltham, 2005; Smedsrud & Jenkins, 2004; Svensson & Omstedt, 1994) as well as the ensuing accretion and ablation cycles (Galton-Fenzi et al., 2012).

While the importance of sea ice in many of the Earth systems is widely accepted (Aagaard & Carmack, 1989; Barry et al., 1993; Notz & Bitz, 2017), predictive models that capture the full suite of physics occurring within the ice are uncommon and are often traded for simpler parameterizations of its properties. Although computationally less expensive, excluding the microscale processes that in turn shape the macroscale properties of the sea ice layer can drastically reduce the accuracy of these models (Petrich & Eicken, 2017) and prevent effective representation of sea ice in larger Earth systems models (Notz, 2012). Here a one-dimensional, finite difference model of sea ice that includes the multiphase physics described by mushy layer theory as

well as a mechanical, energy-conserving model of platelet ice accretion is presented. What follows is a description of the one-dimensional numerical model (section 2), results from the model's application to sea ice under various oceanic and atmospheric conditions as well as its ability to reproduce field observations (section 3), and a discussion of the model's utility in simulating an array of Earth and planetary ice-ocean environments (section 4).

2. Numerical Model

Sea ice growth is treated as a reactive transport model where water/ice mass, energy, and salinity are conserved in a multiphase framework. The growth of sea ice also accounts for accretion at the ice-seawater interface. An overview of the different aspects of the model is given below; a complete description of the theory employed in the model's design can be found in the supporting information. Appendix A lists all variables used in the text.

2.1. Advection-Reaction-Diffusion Multiphase Model

The model discussed herein utilizes mushy layer theory to simulate the ice-ocean system. This approach uses continuum mechanics to approximate the properties of representative elementary volumes (Feltham et al., 2006; Hunke et al., 2011) and has been implemented in several contemporary sea ice models (Griewank & Notz, 2013; Turner et al., 2013; Turner & Hunke, 2015).

The equations of mushy layer theory ensure the conservation of heat (equation (1)) and mass (equations (2) and (3)):

$$\overline{\rho c}\frac{\partial T}{\partial t} = -\rho_{br} c_{br} w \frac{\partial T}{\partial z} + \frac{\partial}{\partial z}\left(\bar{k}\frac{\partial T}{\partial z}\right) - \rho_{ice} L \frac{\partial \phi}{\partial t} + Q \tag{1}$$

$$\phi \frac{\partial S_{br}}{\partial t} = -w\frac{\partial S_{br}}{\partial z} + \frac{\partial}{\partial z}\left(\bar{D}\frac{\partial S_{br}}{\partial z}\right) - \frac{\rho_{ice}}{\rho_{br}} P_S S_{br} \frac{\partial \phi}{\partial t} \tag{2}$$

$$\frac{\partial w}{\partial z} = \left(\frac{\rho_{ice}}{\rho_{br}} - 1\right)\frac{\partial \phi}{\partial t} \tag{3}$$

where ρ is density, c is specific heat capacity, T is temperature, t is time, w is brine velocity, z is the vertical coordinate, k is heat conductivity, L is the latent heat of fusion for the water to ice phase transformation, ϕ is liquid fraction, Q is any external heat sources such as solar radiation, S is salinity, D is salt diffusivity, and P_S is a partition coefficient used to simulate the incorporation of salt into the solid phase (ice) via precipitation and fractional crystallization. Subscripts *ice* and *br* refer to characteristics of the ice and brine components of the cell, respectively, and variables with the over bar are volumetrically averaged quantities (i.e., for a characteristic y, $\bar{y} = \phi y_{br} + (1-\phi) y_{ice}$).

Equations (1)–(3) contain four unknowns and the system of partial differential equations still needs to be closed. The present model employs an enthalpy method (Huber et al., 2008) to iteratively calculate the liquid fraction of a given unit cell. This is done using the following two equations:

$$H = c_{ice} T + L\phi \tag{4}$$

$$\phi = \begin{cases} 0 & H < H_s = c_{ice} T_m \\ (H - H_s)/L & -if - H_s \le H \le H_s + L \\ 1 & H > H_s + L \end{cases} \tag{5}$$

where H is enthalpy, T_m is the melting temperature, and H_s is the enthalpy if the cell was completely frozen out (enthalpy of solid ice) given its current salinity. The melting temperature is calculated via a linearization of the freezing point depression due to salinity (see supporting information).

There are a number of assumptions implied with the definition of the model. First, the model neglects external heat sources (Q), such as solar radiation. Second, thermal conductivities (k), salt diffusivities (D), and specific heats (c) are taken to be approximately constant for both ice and brine allowing for their removal to outside of the spatial derivatives in the equations for heat and mass conservation (salt diffusivities are assumed to follow Archie's law for ion flow [see supporting information]). Additionally, the partition coefficient (P_S) is set to a constant. These simplifications were made to accelerate the development process and

upon validation of the utility of the model full expressions for these variables will be included (see section 4.2 for details). Finally, we assume that the discretization cells are in local thermodynamic equilibrium, which is shown to be appropriate for sea ice (Feltham et al., 2006). The one-dimensional model can then produce spatially and temporally varying profiles of temperature, salinity, brine velocity, liquid fraction, precipitated/fractionally crystallized salt, and total salt content.

2.2. One-Dimensional Density-Driven Convection Parameterization

Due to the reduced ability of crystalline ice to incorporate salt into its lattice, as a volume of sea ice solidifies its interstitial brine becomes increasingly saline. With a temperature gradient present from the ice-atmosphere interface to the ice-ocean interface, there inevitably forms a similar gradient in salinity of the interstitial brine (based on the liquidus relationship of seawater and the assumption of local thermodynamic equilibrium). This gradient produces a density instability that results in convection through the porous portion of the ice, leading to desalination of the ice column.

In the one-dimensional regime, the phase change driven brine velocity of the model outlined above is insufficient to expel enough salt to match field and experimental observations. This leads to supersalination of the upper ice layers and ultimately unphysical numerical simulations. One-dimensional models cannot explicitly simulate the gravity driven convection that occurs in the porous layers of the forming ice as it is an inherently multidimensional process. This process has been shown to be the primary mode of sea ice desalinization aside from surface flushing (Notz & Worster, 2009). Thus, a parameterization of density-driven convection is implemented. These types of parameterizations have been investigated before (Griewank & Notz, 2013; Turner et al., 2013) and the model presented in Griewank and Notz (2013; from here on GN2013) is closely followed here (see supporting information for details).

The one-dimensional parameterization models convective overturn through brine channels as a linear function of the local Rayleigh number. GN2013 give the mass of brine transported out of an ice layer j as

$$br_j^{\downarrow} = \alpha\left(Ra_j - Ra_c\right)dz^3 dt = \alpha\left(\frac{g\rho_{sw}\beta\Delta S_j \tilde{\Pi}_j h_j}{\kappa\mu} - Ra_c\right)dz^3 dt \tag{6}$$

where α is a constant of proportionality optimized by GN2013 using the Levenberg-Marquardt algorithm to be 1.56 $\times$ 10^{-3} kg/(m^3 s), Ra_j is the Rayleigh number of the jth layer, Ra_c is the critical Rayleigh number, dz and dt are the spatial and temporal discretization sizes, respectively, g is acceleration due to gravity, ρ_{sw} is the density of seawater, β is a density coefficient describing the relationship between density and salinity, ΔS_j is the difference in salinity of the brine from ambient seawater, h_j is the height of the jth layer above the basal surface of the ice, κ is the thermal diffusivity of seawater, μ is the kinematic viscosity of seawater, and $\tilde{\Pi}_j$ is the minimum permeability of any layer between the jth layer and the basal ice surface. The permeability function given by GN2013 is utilized (supporting information, equation (S9)), but a critical porosity cutoff is implemented to prevent drainage from layers containing low liquid fractions (here $\phi < 0.05$ (Golden et al., 2007) results in a layer's fluid transport being shut off). There is disagreement in the literature as to whether such a porosity cutoff exists for sea ice (Golden et al., 2007; Griewank & Notz, 2013; Oertling & Watts, 2004), and additional permeability-porosity relationships are investigated in section 4.3.

Heat and salt are transported via these brine flows. Thus, alongside the one-dimensional advection-reaction-dispersion model, for every time step, the heat and salt transported via the density-driven convection parameterization is calculated using the brine flows, producing a heat and salt sink/source term for each layer j. The heat and salt sink/source term is utilized in equations (1) and (2), respectively, to simulate the evolution of the forming ice with the inclusion of one-dimensional parameterized density-driven convection. Equations (1) and (2) now become

$$\overline{\rho c}\frac{\partial T}{\partial t} = -\rho_{br}c_{br}w\frac{\partial T}{\partial z} + \frac{\partial}{\partial z}\left(\bar{k}\frac{\partial T}{\partial z}\right) - \rho_{ice}L\frac{\partial \phi}{\partial t} + Q_{source} \tag{7}$$

$$\phi\frac{\partial S_{br}}{\partial t} = -w\frac{\partial S_{br}}{\partial z} + \frac{\partial}{\partial z}\left(\bar{D}\frac{\partial S_{br}}{\partial z}\right) - \frac{\rho_{ice}}{\rho_{br}}P_S S_{br}\frac{\partial \phi}{\partial t} + S_{source} \tag{8}$$

where the *source* terms are calculated using the previous time step's liquid fraction, temperature, and salinity values. These new source terms account for the one-dimensional advection terms' inability to simulate convection.

2.3. Platelet Ice Accretion

The accretion of frazil and platelets once again alters the ice-ocean interface. The goal of this phase of the model is to construct a method for parameterizing platelet ice accretion that can be used in a continuum scale representation of sea ice formation. Such a model would be capable of testing the sensitivity of floating ice evolution to variations in platelet ice characteristics and the impact of variable supercooling on ice and platelet layer thickness. The model calculates an accretion rate in two steps. First, the enthalpy method described above is utilized to predict the frazil/platelet production rate in the water column (this step is thermodynamically independent of the reactive transport model described in section 2.1 and is used solely to predict the volume of ice nucleated and grown in the water column due to supercooling). Second, for a given platelet ice crystal size distribution a vertical mass flux is calculated based on a force balance of rising frazil/platelets (for a 1 cm [radius] platelet with a rise velocity of ∼0.02 m/s the Reynolds number is ∼114).

For a given amount of supercooling (e.g., 40 mK for the upper water column of McMurdo Sound; Hughes et al., 2014; Robinson et al., 2014) and a given time discretization (e.g., $dt = 50$ s) the enthalpy method is used to calculate the change in ice volume fraction over a specified spatial grid node (e.g., $dz = 1$ cm). Next a prescribed probability distribution is used to represent the sizes of the platelets present in this layer. This is a parameter space that will be varied as the actual population distribution of platelet sizes may be broad and is not well constrained (McFarlane et al., 2014; see section 4.3.1). The next step in acquiring an accretion rate is calculating the rise velocity of the suspended platelets. This is done by balancing the buoyancy force and the drag force on a given platelet, assuming platelets do not interact hydrodynamically with each other, and solving for velocity:

$$\vec{F}_B = \vec{g}\,(\rho_{sw} - \rho_{ice})\pi R^2 h = \frac{1}{2}\rho_{sw} v^2 c_d A = \vec{F}_D \tag{9}$$

where $\vec{F}_B$ is the buoyancy force, $\vec{F}_D$ is the drag force, R is the platelet radius, h is the platelet height, v is the rise velocity, c_d is the drag coefficient, and A is the platelet cross sectional area. To rewrite the solution in terms of the platelet radius, R, an aspect ratio, $a_s = h/R$, is introduced. This assumes that the platelets exist as flattened cylinders. This is done for simplicity, as the complex and unique geometry of the suspended ice crystals will undoubtedly result in associated complex rise dynamics (McFarlane et al., 2014). The aspect ratio and drag coefficient are variable parameters that are not well constrained by observations. Sensitivity analysis was conducted to investigate the feasible limits of platelet dynamics and accretion, and the effects of platelet properties on the overlying ice evolution (see section 4.3.1). Substituting the aspect ratio into equation (9) and solving for velocity gives

$$\vec{v} = \sqrt{\frac{2\vec{g}\,(\rho_{sw} - \rho_{ice})a_s R}{\rho_{sw} c_d}} \tag{10}$$

An example of a population distribution and its corresponding platelet size-dependent rise velocity can be found in Appendix B. Multiplication of the rise velocity distribution by the population distribution produces a platelet flux distribution that, when integrated, will give the solid fraction flux passing through a horizontal plane in the water column (Appendix B). This solid fraction flux is used as the buoyancy driven accretion rate. During a simulation, for a given time step dt, the advection-reaction-diffusion model and the one-dimensional convection model are allowed to stabilize, then an amount of solid ice, equal to the accretion rate times the time step dt, is added to the lowest multiphase layer. The only exception to this is when the bottom multiphase layer is below a preset critical porosity, ϕ_c (i.e., the combined solid fraction [congelation ice formed via heat loss to the atmosphere + accreted platelet ice] at the ice-seawater interfacial node is greater than $(1 - \phi_c)$). In this case the ice is added to the liquid layer below it. This ensures that the simulated subice platelet layer does not exceed observed solid fractions by accretion alone (typically anything less than $\phi \cong 0.7$).

3. Results

In addition to the simulation of realistic sea ice cores (3.1) the model was run under simplified conditions to simulate the dynamics of pure substance melting (the Stefan problem) to validate its accuracy against the known analytical solution. The numerical model produced melting front propagations and liquid fraction

profiles that agree well with the analytical solution. Additionally, sensitivity studies were performed to test the capability of the model to handle a wide range of parameter space and to investigate the effects observationally unconstrained parameters may have on the properties and evolution of forming sea ice. Modifying the population distribution and variables governing the dynamics of forming and accreting platelet ice appreciably affected the growth rate of the forming sea ice. Varying the relationship coefficient (α) dictating the efficiency of brine expulsion from the growing sea ice impacted both growth rates and overall salt content of the forming ice. The permeability-porosity relationship utilized is shown to drastically affects the

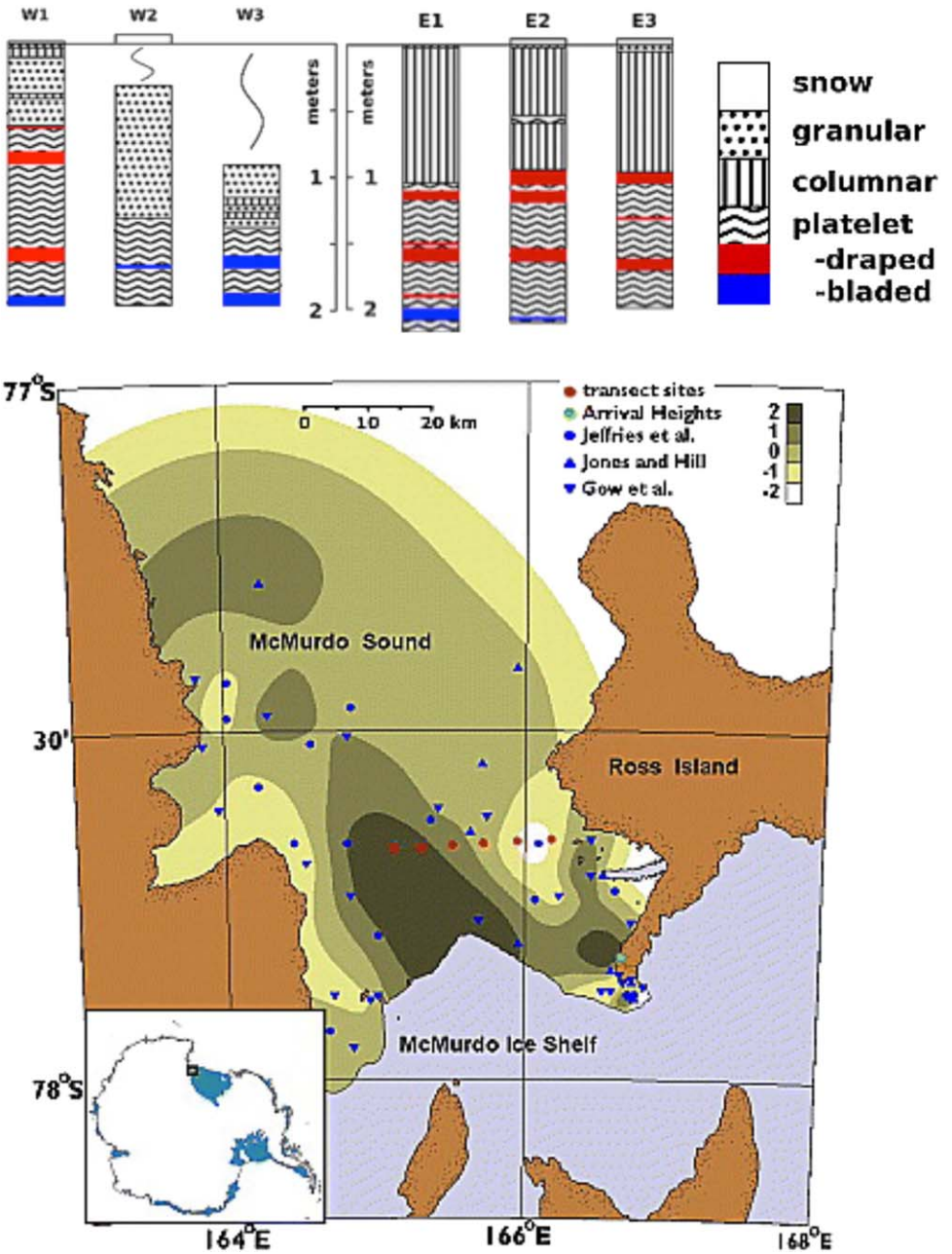

Figure 1. Adapted from Dempsey et al. (2010). (top) Depiction of the results of the structural analysis carried out on the extracted sea ice cores, highlighting variations in crystal texture with depth. (bottom) Geographical representation of the study location. The cores analyzed by D10 are shown in red, and progress from left to right in line with the above ice core structure diagram. The white to brown shading of the sound is a measurement of relative platelet ice abundance utilizing the D10 results and other historical studies. This can be used as a proxy for the geometry and intensity of the ice shelf water plume.

chemical characteristics of growing sea ice. Finally, changing values of the partition coefficient (P_S) minimally affected the salt content in the simulated ice. A full description of the Stefan problem and sensitivity analysis can be found in the supporting information and section 4.3, respectively.

3.1. Sea Ice Core Simulations

The model was used to simulate sea ice growth under realistic environmental conditions for the McMurdo Sound (Antarctica) to both test the model, and to investigate the role of platelet accretion in sea ice growth. The McMurdo runs implemented environmental conditions described by Dempsey et al. (2010; from here on D10) to reproduce three ice cores extracted and analyzed in the Austral summer of 2007. D10 extracted a total of six sea ice cores from a west to east transect just north of the McMurdo Ice Shelf terminus, an area heavily influenced by a supercooled ice shelf water plume (Dempsey et al., 2010; Robinson et al., 2014). The cores were analyzed for structural and compositional properties, resulting in profiles of ice texture (columnar, granular, and incorporated platelet ice) and salinity. Here we focus on three distinct cores (using the vernacular from D10, see Figure 1), W1, W3, and E-type (E1–E3), chosen for the theorized disparate conditions under which they formed. The western cores are thought to have formed in a region more heavily influenced by the buoyant ice shelf water plume, resulting in a higher degree of localized supercooling in the underlying water column, producing the greater relative platelet ice abundance observed in their respective ice cores. The three core types also display unique predicted freeze over dates, constrained by satellite data, allowing for investigation of how surface temperature impacts sea ice characteristics.

3.1.1. Initial and Boundary Conditions

For each run a one-dimensional column of seawater (34 ppt, 100% liquid fraction, fluid at rest) just above its freezing point (−1.9°C) is simulated. From this point forward the bottom boundary is refreshed to this

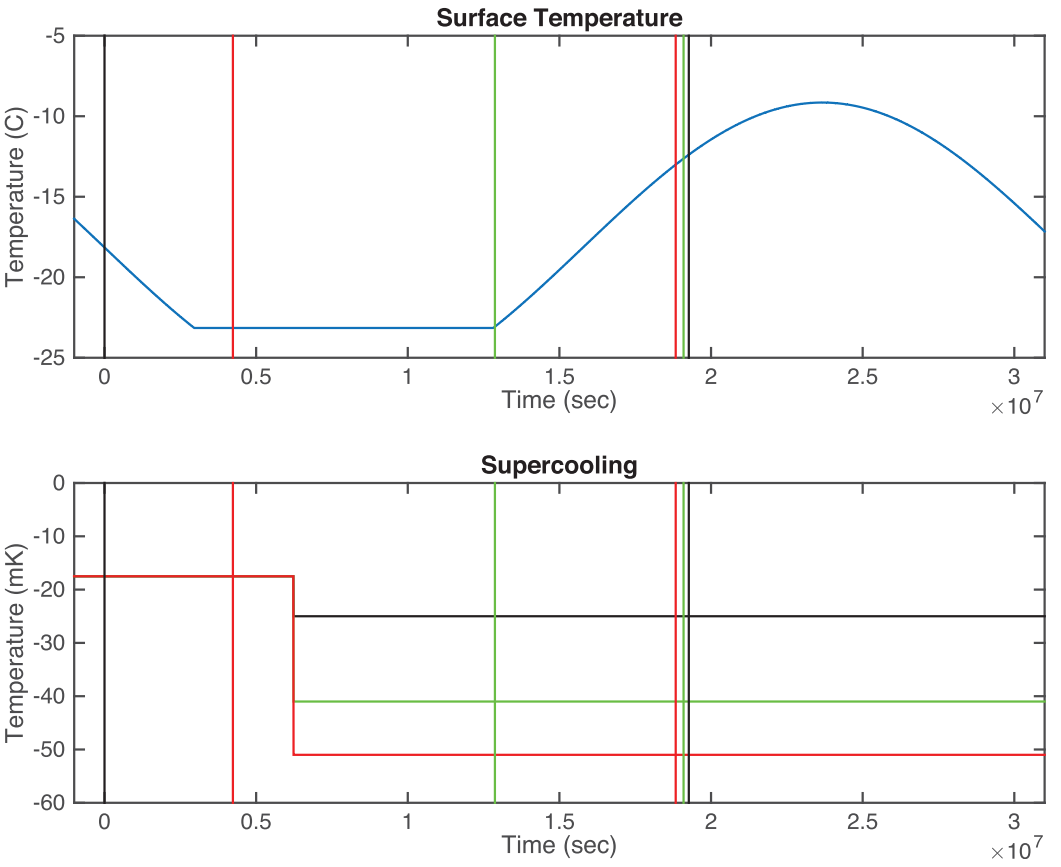

Figure 2. Plots showing the boundary conditions used during the model runs. (top) Surface temperatures used for the no-slip upper boundary (blue). E-type, W1, and W3 ice core start and stop times can be seen in black, red, and green, respectively. (bottom) Supercooling values used to force the formation and accretion of platelet ice throughout the model runs. Color coded as above, vertical lines represent start and stop times and the variable supercooling can be seen after $\sim 6 \times 10^6$ s.

Table 1
Comparison of Simulated Ice Cores and Field Observations: Summary of Boundary Conditions, Model Results, and Empirical Observations of Ice Core Structure

Ice core	W1	W3	E-type
Supercooling (model) (mK)	17.5–50	17.5–40	17.5–25
Congelation-platelet transition (D10) (cm)	60	46	94–104
Congelation-platelet transition (model) (cm)	61	48	102
Total core length (D10) (cm)	197	105	199–218
Total core length (model) (cm)	192	105	196
Total run duration (model) (day)	169	72	223
Total freeze duration (D10) (day)	113–169	55–72	150–260

ambient seawater temperature and salinity. The top boundary is subject to a simplification of a seasonally varying atmospheric temperature (Dirichlet boundary condition, see Figure 2). Each core's predicted freeze over date acts as the initial surface temperature and it then progresses per the temperatures given in Figure 2. Throughout the run, the top surface is simulated as being in contact with an atmosphere containing no liquid fraction at the given surface temperature. The bottom boundary is simulated as a free slip surface in contact with ambient seawater (34 ppt, 100% liquid fraction, −1.9°C, no fluid velocity) that can exchange heat, salt, and fluid into and out of the model domain.

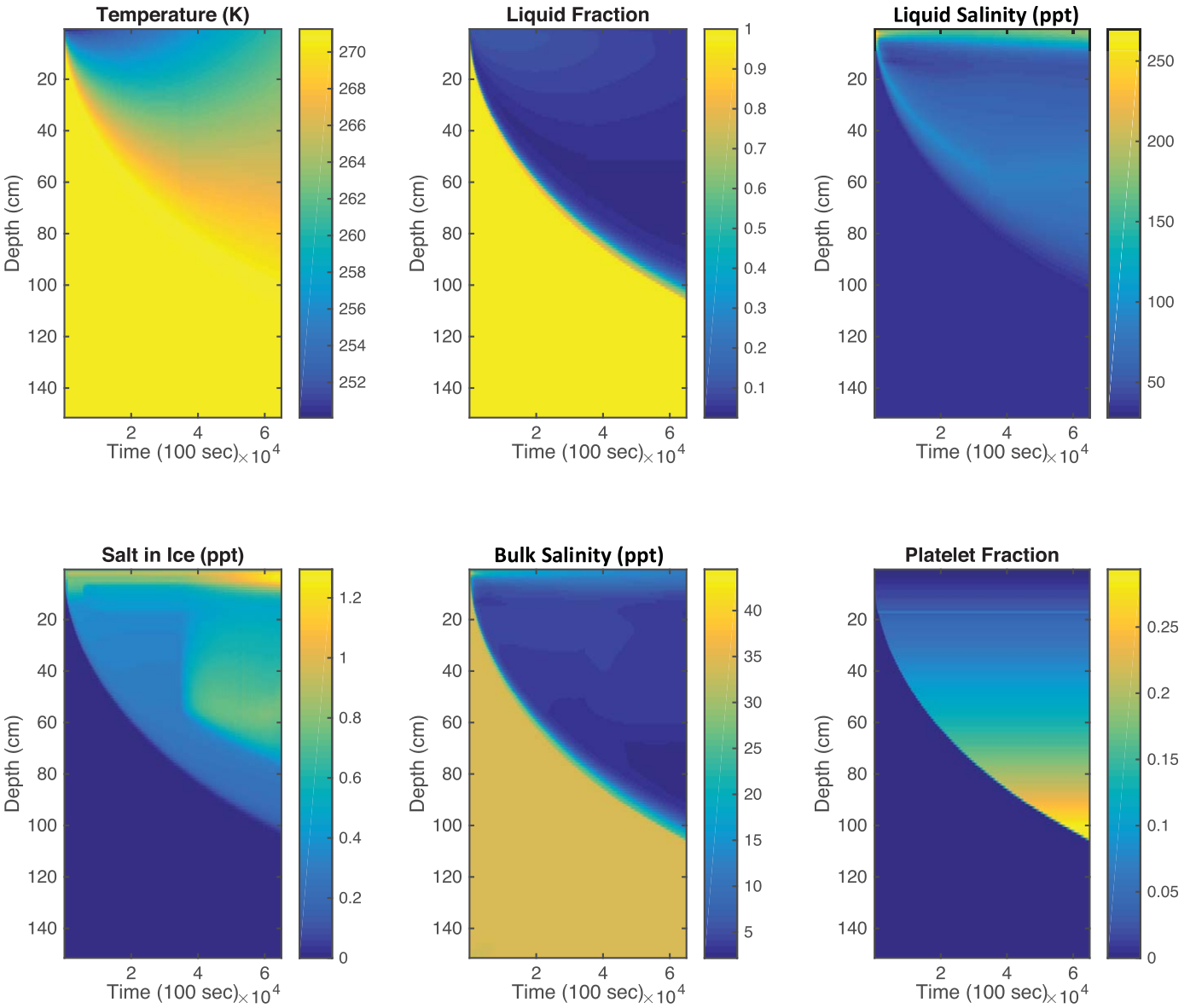

Figure 3. Density plots displaying the entire numerical simulation of the W3 ice core. The notable jump in the "Salt in Ice" plot is associated with the minimum permeability cutoff imposed in the gravity drainage parameterization, which effectively traps salt in pockets where it precipitates out of solution. The brief jump in the "Platelet Fraction" plot at ~18 cm is associated with the onset of convection as it briefly impedes the propagation of the freezing front. This onset can be seen in the "Salinity" plot as well, there as a decrease in salinity when the sea ice reaches this critical thickness.

The model does not allow for the vertical transport of solid ice through the model domain, therefore to simulate platelet formation and transport in the water column an additional thermal profile tracking supercooling is kept separately. This ensures that immobile solid fraction does not form throughout the water column during simulations but is utilized alongside the enthalpy method to calculate the platelet ice accretion rate (supporting information equations (S.13)–(S.16)) computed at each time step. The oceanic boundary is forced by a simple spatially and temporally varying amount of supercooling, simulating an ice shelf water plume impinging upon the base of the sea ice. The seasonal supercooling for the W1, W3, and E-type ice cores can be seen in Figure 2, where the cores are subject to an ambient supercooling of 17.5 mK until the central portion of the sound begins to freeze over at which point the supercooling is amplified in line with the relative platelet ice abundance presented in D10 (see Figure 1). The supercooling in the central portion of the plume is set to 50 mK (in agreement with maximal supercooling values measured in the area; Hughes et al., 2014; Robinson et al., 2014), falling off to 40 mK by the W3 core, and finally 25 mK for the E-type cores. Here the focus is to show the model's ability to accommodate variable supercooling and demonstrate the effects it has on ice core structure, while improvements to plume geometry and temporal variability and their effects on sea ice evolution are left for future applications of the model.

3.1.2. Simulated Ice Cores

Model runs for each core type were carried out utilizing the estimated freeze over dates, simulation durations, and supercooling values listed in Table 1 (also listed are the range of freeze over dates predicted by D10 and the dates the cores were extracted). Color density plots of the physical, chemical, and thermodynamic profiles produced by the model are shown in Figure 3, which displays the entire numerical simulation of the W3 ice core. These profiles allow for high temporal ($dt = 50$ s) and spatial ($dz = 1$ cm) resolution of the evolution and dynamics occurring during the formation of congelation sea ice affected by platelet ice accretion. The model can accurately simulate variable boundary and initial conditions, the realistic reactive transport phenomenon observed in natural sea ice, and the inclusion of platelet ice accretion. A comparison of the vertical properties of the ice cores simulated during the model runs to the observations made by D10 is given in Figure 4. Layers demarcated as "platelet ice" have more than 10% of their volume fraction made up by accreted platelet ice, in line with the ice core structure characterization used by D10. Throughout the simulations, the only parameters that differ between the three core types are the level of supercooling in the underlying water column and the freeze over/extraction dates, all other free parameters (drag

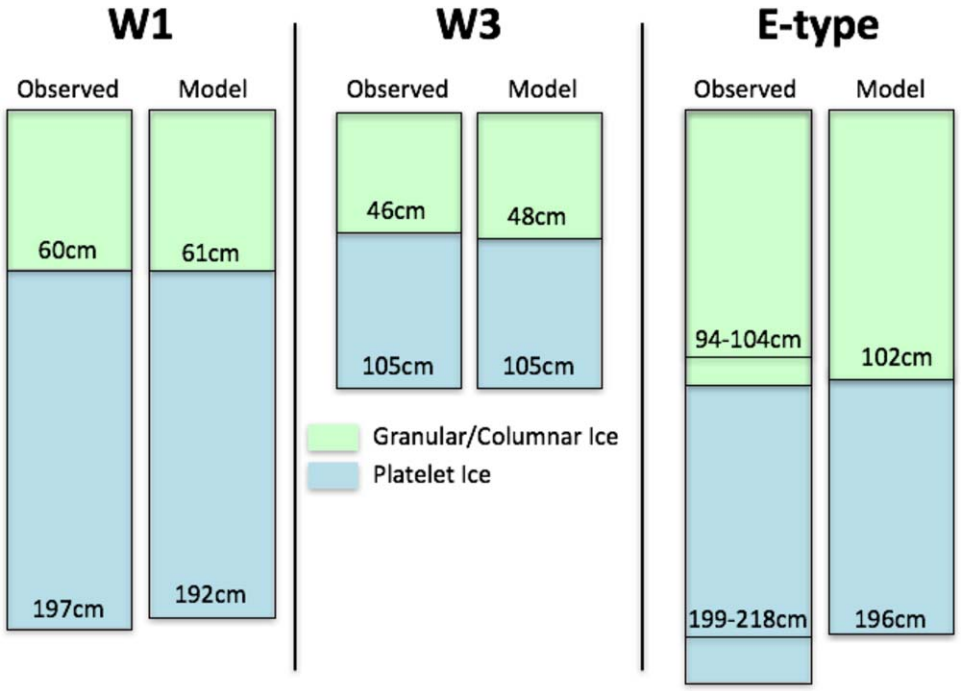

Figure 4. Pictorial representation of the model results (full profiles depicted in Figures 5–7) for the E-type, W1, and W3 cores and a comparison to the observations made by D10.

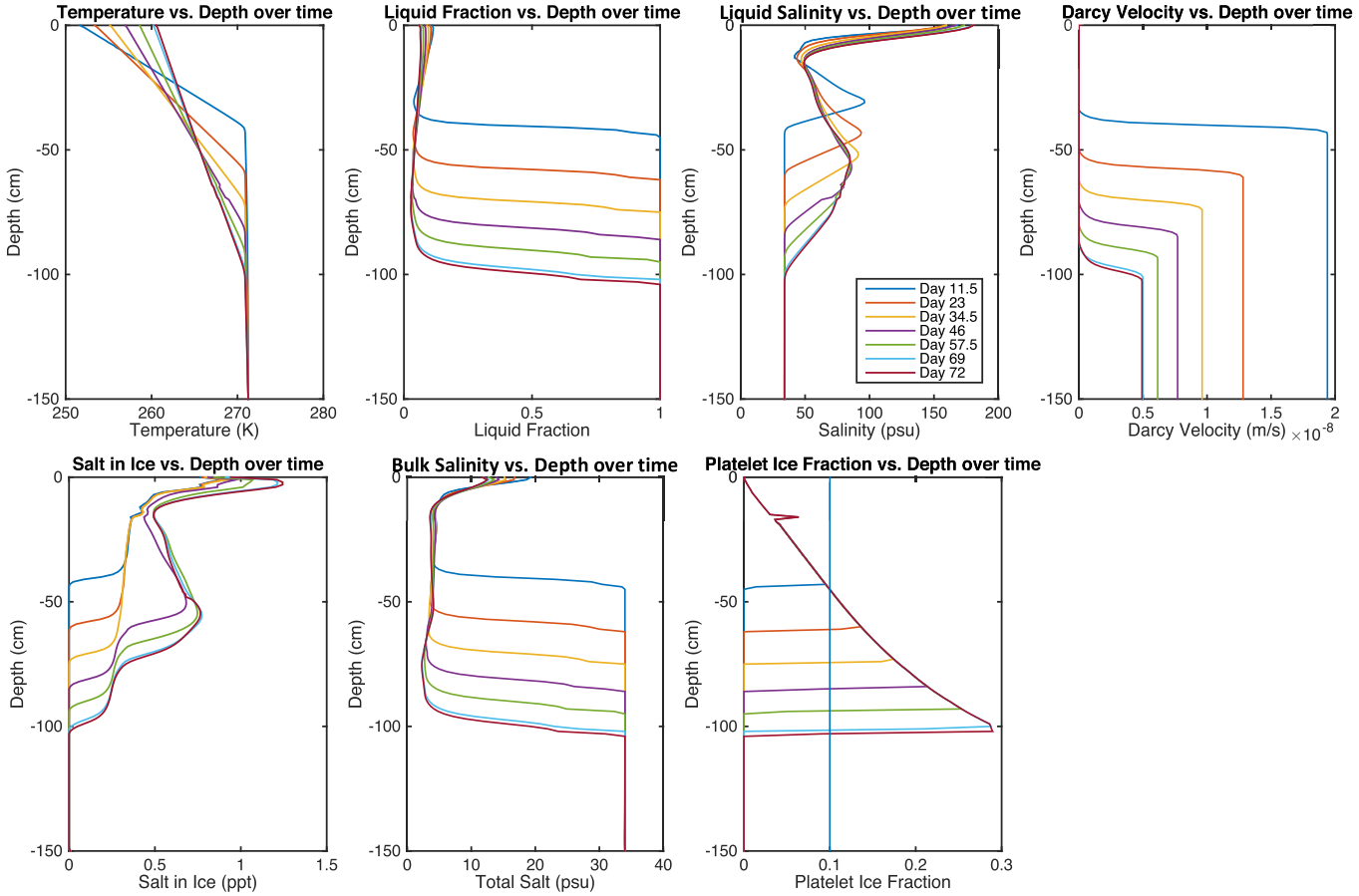

Figure 5. Temporally varying vertical profiles output by the model for the W3 ice core. Vertical line in the Platelet Ice Fraction plot represents 10% volume fraction of platelet ice.

coefficient, convection parameterization coefficient, platelet aspect ratio, etc.) are chosen a priori using values in the median of realistic parameter space and are held constant for all runs (see Appendix A for parameter values). The model results are in excellent agreement with the observations of D10, utilizing conditions well within the predicted range for McMurdo Sound (Dempsey et al., 2010; Hughes et al., 2014; Robinson et al., 2014). Temporally varying ice core profiles of temperature, salinity, liquid fraction, and total salt content can be extracted to easily visualize the yearlong evolution of the ice at each location (W1, W3, and E-type), examples of which can be seen in Figures 5–7. The thermal, chemical (salinity and total salt content), and structural (liquid fraction, ice texture—congelation versus platelet ice) profiles are in good agreement with both observation and theory: these reveal a primarily conductive temperature profile, a low but nonzero porosity ice structure with a highly porous basal layer, and a progressively desalinating "c-shape" total salinity profile (Malmgren, 1927).

4. Discussion

4.1. Comparison to Field Observations

The profiles produced by the numerical simulation agree well with the observations made by D10. In nearly all cases both the qualitative structure of the salt content, temperature, and porosity profiles, as well as their simulated values, are in line with those seen in the actual cores extracted during the D10 study (or theory and comparable studies for properties not measured in D10). In the case where the quantitative values do not mirror those seen empirically, namely total salt content, modifying free parameters in the numerical model can remedy the minimal discrepancy (see section 4.3).

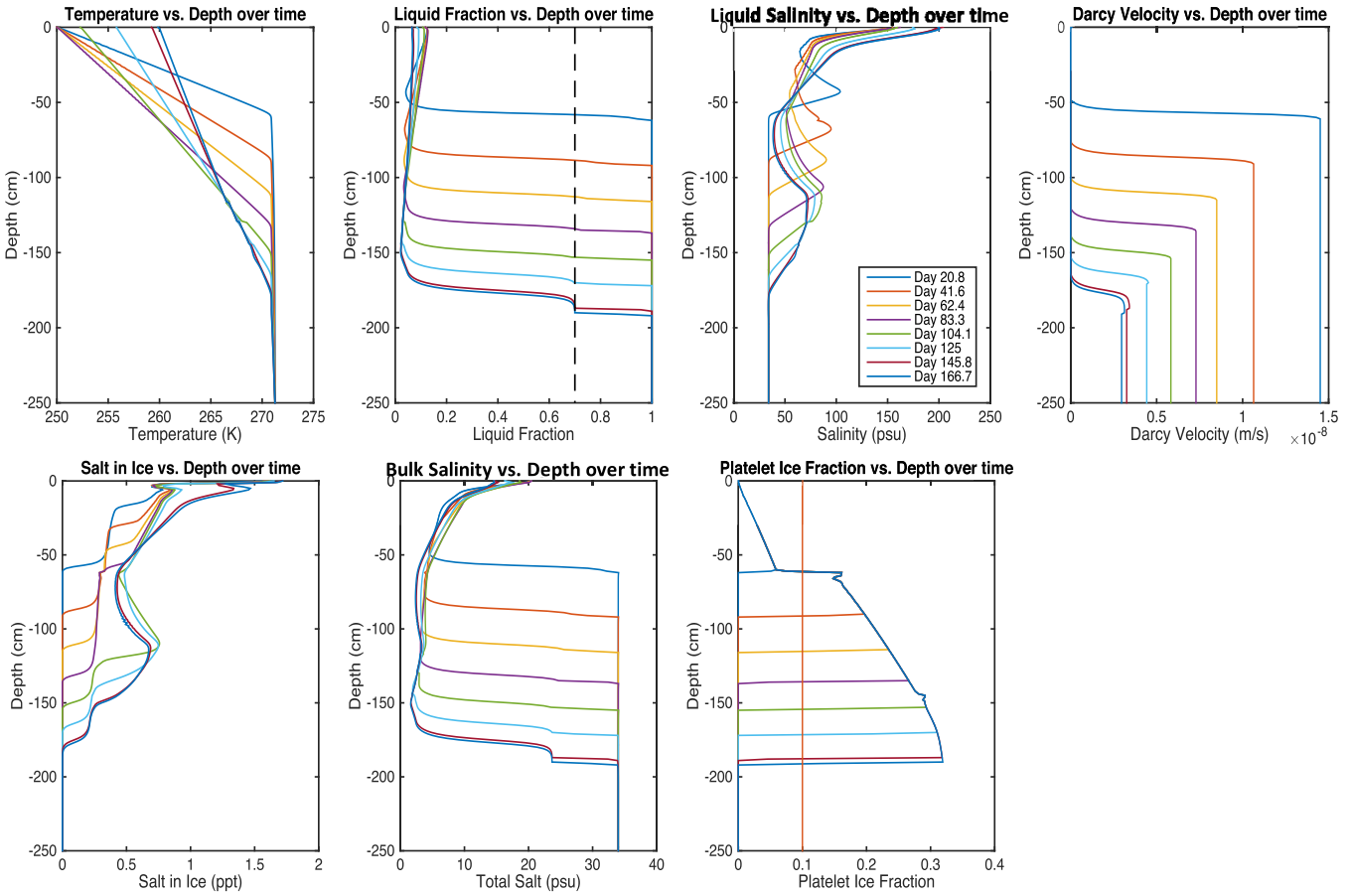

Figure 6. Temporally varying vertical profiles output by the model for the W1 ice core. The dotted line in the liquid fraction plot denotes the critical porosity of 0.7 set for the accreting platelet ice. Vertical line in the Platelet Ice Fraction plot represents 10% volume fraction of platelet ice.

4.1.1. Structure and Temperature Profiles

The simulated ice core stratigraphies both qualitatively and quantitatively agree with the structural properties seen by D10. A layer of congelation ice is formed early in the season when temperature gradients at the basal surface of the ice are high. Even in the presence of a supercooled water column the advancing ice-ocean interface propagates at a rate that quickly consumes any accumulating platelets, leaving a granular or columnar texture as the dominant crystal fabric. This can be seen in Figures 3–7 where a low platelet fraction persists throughout the upper portion of the ice. Later in the season when surface temperatures have begun to increase and the sea ice growth from heat loss to the atmosphere slows the crystal fabric becomes dominated by incorporated platelet ice. This occurs in situations with variable supercooling (as in cores W1 and E-type, where an amplification in supercooling is initiated at a preset date) and with constant supercooling (as in core W3, that was subject to 40 mK of supercooling throughout its formation). During the spring-summer season, when the ice cores were extracted, the temperature gradients at the basal surface of the ice were at their lowest and if sufficient supercooling persists, a subice platelet layer forms.

A subice platelet layer can be seen beginning to form for the W1 core in Figure 6. This core has the highest supercooling (50 mK) and thus has the highest propensity for forming this layer. It is characterized in the numerical model output by the sharp downward propagation of an ice layer with a porosity equal to the preset critical porosity, ϕ_c, demarcated by the dashed line in Figure 6. There are some instances where simulated ice cores have total lengths and/or congelation-platelet ice transitions that minimally vary from observations. These variations are only a few centimeters and modifying the environmental parameters (e.g., surface temperature, supercooling, freeze duration, and platelet size distribution) could quickly remove any discrepancies (see section 4.3).

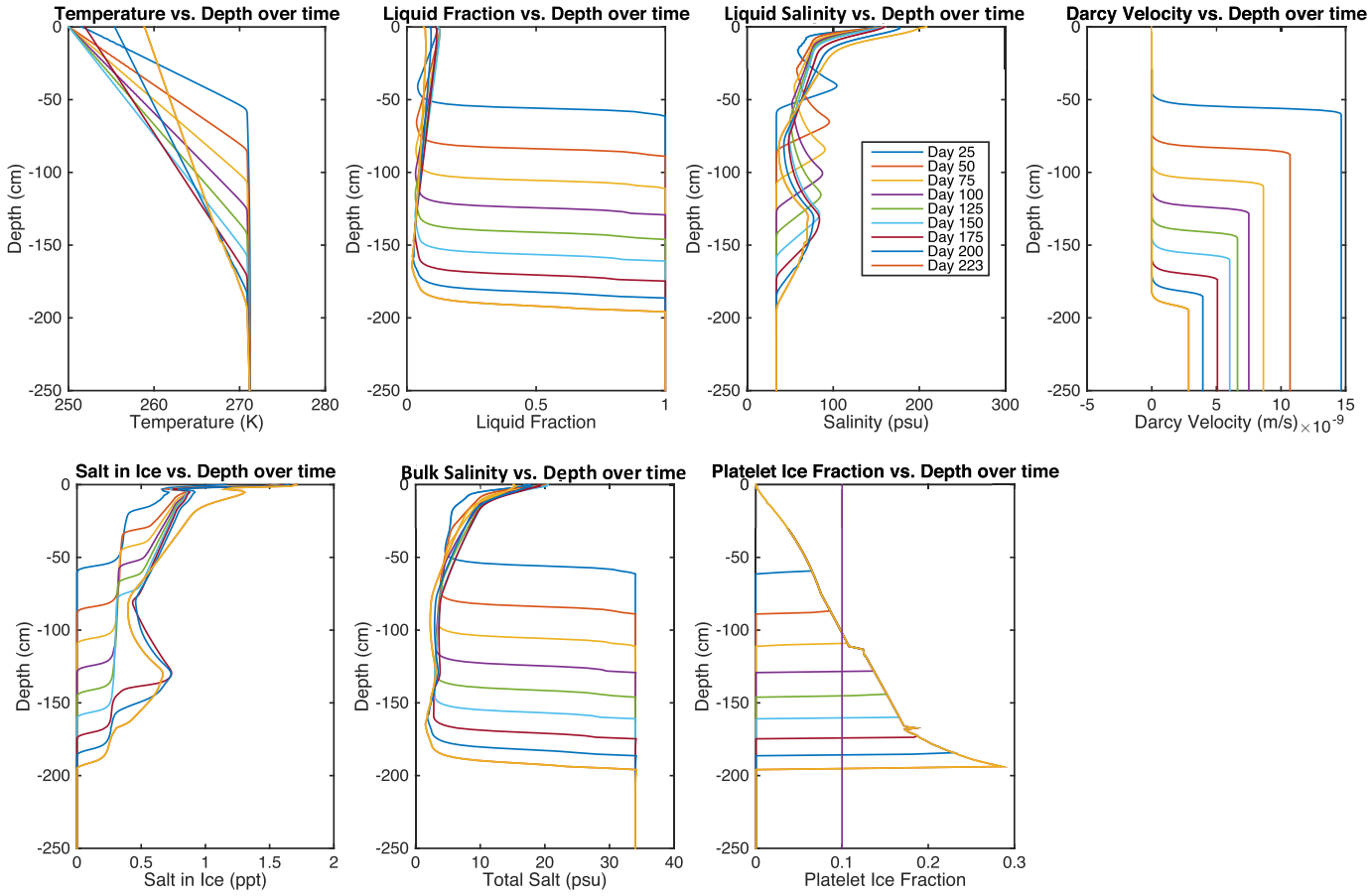

Figure 7. Temporally varying vertical profiles output by the model for the E-type ice core. Vertical line in the Platelet Ice Fraction plot represents 10% volume fraction of platelet ice.

Simulated temperature profiles agree with thermodynamic predictions as well as field measurements using thermistor arrays frozen into growing sea ice (Perovich et al., 1997; Petrich & Eicken, 2017; Thomas, 2017; Thomas & Dieckmann, 2009). An equilibrated conductive profile is expected due to the high thermal conductivity of ice (compared to brine or seawater). This allows the ice layer to reach thermodynamic equilibrium at a faster rate than the ice-ocean interface propagates, leading to a linear temperature profile between the surface and the ambient ocean. The agreement between the model and both theory and observations is shown in the temperature profiles of Figures 5–7.

4.1.2. Salt in Sea Ice

The total salt profile in young first year sea ice (before surface melting initiates) typically has a "c-shape" profile with increased salt concentrations at the ice-atmosphere and ice-ocean interfaces. While this has been well documented by field observations for nearly a century (see Malmgren, 1927), numerical models of sea ice struggle to reproduce total salt values without assuming an a priori salt distribution, and frequently underestimate the bulk salinity of sea ice (Turner & Hunke, 2015). The models utilizing a priori salt distribution parameterizations can more closely reproduce total salt content values for some ice cores, but inevitably not for others, as they take no account of how the environment effects the salt distribution within the ice. Sensitivity analyses reveal that the local environment and the ensuing ice dynamics uniquely determines the chemical profile of the ice that forms (see section 4.3 and Figures 10 and 11). The goal of successfully incorporating sea ice models into Earth systems models relies on the interaction between the ice, the ocean, and the atmosphere, thus in this model we choose to forego a priori assumptions and utilize environmental conditions and conservation equations to determine the total salt profiles. The model results produce the characteristic "c-shape" profiles quite well, but suffer from an underestimation of total salt, with average bulk salinities 1.63–3.27 ppt below those measured by D10 (likely due to the lack of constraint

on a number of variable parameters—see section 4.3). Most importantly, these results highlight the need to constrain the dynamics that dictate brine motion throughout the ice, namely gravity drainage. Heterogeneous brine pocket/channel distribution, dead-end conduits, capillary forces, and permeability-porosity relationship errors are all factors that could reduce brine flux out of the forming ice, and in turn increase total salt content relative to the idealized case modeled here.

4.2. Model Function and Applicability

The ice core simulations help constrain which conditions are capable of producing the ice stratification observed in the D10 study, allowing us to better understand ice shelf-ocean-sea ice interactions. These solutions are not unique, as a different selection of boundary conditions and environmental forcing could conceivably reproduce the same ice core stratigraphy. The model is not intended to be a forensic reconstruction of atmospheric and oceanic conditions during the time of freezing, but instead to be a predictive simulation of sea ice thickness and properties under the influence of known environmental forcing, including platelet accretion due to oceanic supercooling. Additionally, the model includes the full suite of multiphase physics occurring within the ice layer, which is imperative in accurately capturing the microscale physics, and in turn the macroscale properties, of sea ice.

The model, in its current state, already lends itself to a variety of applications. Large-scale sea ice models typically do not include the effects of supercooled waters and platelet ice, yet a large portion of fast ice around Antarctica is likely affected by these processes. The platelet abundance map of Dempsey et al. (2010; seen in Figure 1) suggests that the ice shelf water plume emanating from beneath the McMurdo Ice Shelf likely impacts sea ice up to 80 km from the ice shelf front, meaning thousands of square kilometers of sea ice in McMurdo Sound alone are potentially modified by platelet ice accretion. To test the role of platelet ice accretion in stimulating sea ice growth, ice growing under identical conditions but subject to *no* supercooling was simulated and compared to the supercooling case. These results are shown in Figure 8. The discrepancy between the two scenarios amounts to a 15 cm difference in sea ice thickness, a $\sim$14% variability. This comparison shows that platelet ice accretion has the potential to drastically alter the thickness and mass balance estimates of an extensive area of sea ice. These modified estimates have the potential to improve the accuracy of not only sea ice models but also large-scale models of the cryosphere, ocean, and climate that hope to incorporate the dynamics and effects of sea ice.

Another quantity explicitly produced during simulations of the model is brine flux out of the growing ice layer. This influx of hypersaline water into the ocean is a catalyst for the production of high salinity shelf water and also affects buoyancy driven circulation of the Southern Ocean (e.g., Goosse & Fichefet, 1999). An increasing number of ocean simulations include this source of dense, saline water in their model architecture. The multiphase platelet ice model presented here could provide accurate source terms for these ocean models and improve the sea ice component of coupled ice-ocean models.

While based on the high thermal gradient conditions in sea ice, the model is primed to simulate dynamics occurring beneath Antarctic ice shelves as well. Marine ice forms through a similar accretion process, although with reduced supercooling values due to the waters slow ascension along the underside of the shelves (Galton-Fenzi et al., 2012; Khazendar & Jenkins, 2003). The model can already simulate the low temperature gradients at the basal surface of ice shelves and can be used to reproduce multiple years of marine ice accretion and ensuing dynamics. While models exist that simulate the basal accretion and ablation of ice shelves, these models do not simulate the multiphase nature of the accreting marine ice, which could better constrain its properties (thermal, chemical, and physical) and will dictate the solute flux into the top layer of the water column. Understanding the formation and evolution of marine ice is crucial to understanding the mass redistribution of ice shelves, the impact it may have on stabilizing these floating ice masses, how marine ice may impact sea ice formation, and the effects a changing climate has on our world's meteoric ice budget.

4.3. Sensitivity Analysis

Several variables can potentially affect the output of the simulation, given the complexities considered here. Additionally, due to limited observational data, the values of many relevant variables are not well constrained. Here key variables are discussed and sensitivity studies are presented that demonstrate the impact these variables have on the evolution of the overlying ice.

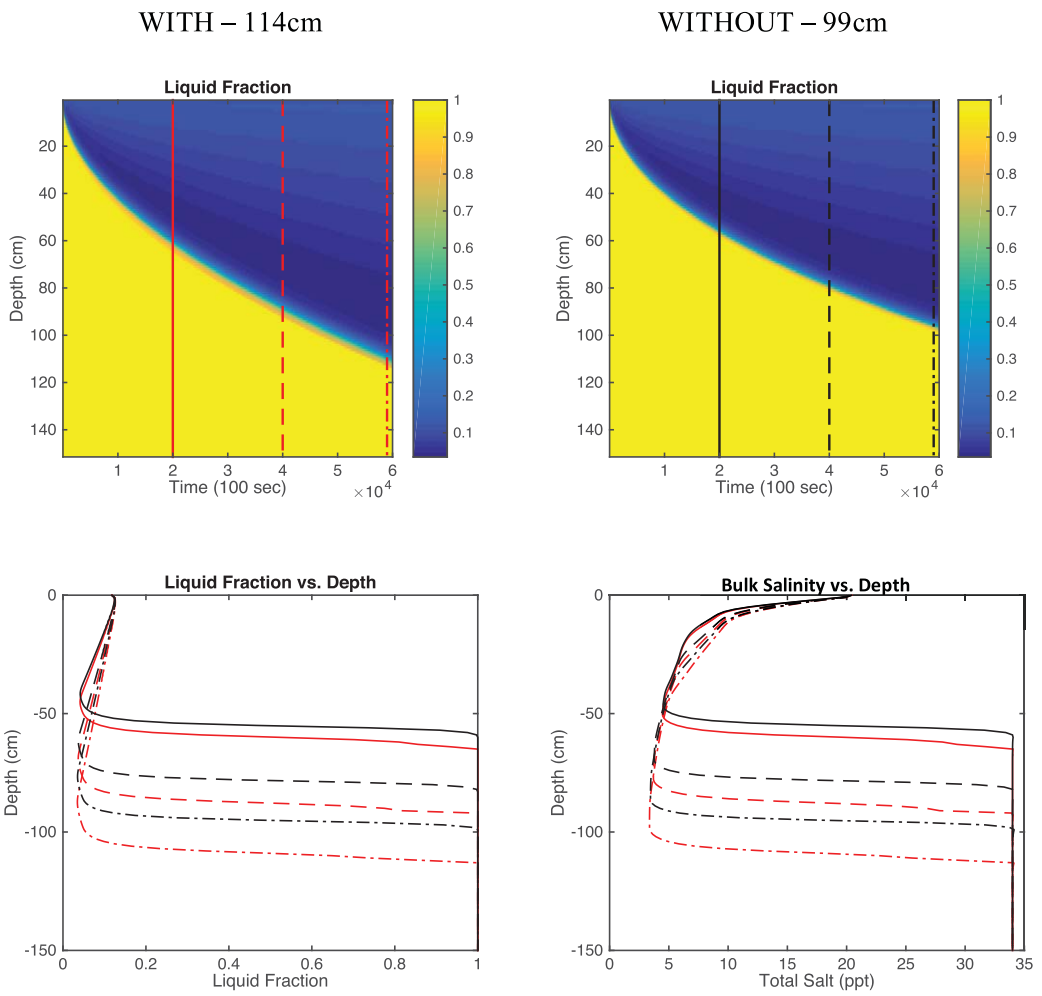

Figure 8. (top) Density plots showing the output of two identical model runs, save for the application of a 40 mK supercooled water layer to the lower portion of the left plot. (bottom) Liquid fraction and bulk salinity evolution for both scenarios (line varieties correspond to vertical lines in the density plots).

4.3.1. Platelet Ice Dynamics

Likely the least constrained portion of the model is the production and evolution of frazil/platelet ice crystals in the water column and their accretion onto the basal surface of the sea ice. The enthalpy method guarantees conservation of energy and thus accurately accounts for the mass of ice produced, however how this ice mass is distributed among platelet shapes and sizes in the water column is largely unconstrained. Crystals have been documented to range from millimeters to centimeters, possessing "high" aspect ratios (proposed ratios range from 1:10 to 1:100; McGuinness et al., 2009), and the overall size distribution has at most been qualitatively documented. All of these properties can influence the overall ice flux onto the overlying ice and thus the overall ice thickness. The drag coefficient of the rising platelets (equation (9)) is an additional unconstrained parameter, although it likely varies over a much smaller magnitude. Finally, the packing efficiency of the rising crystals, governed by ϕ_c, can influence the thickness of the subice platelet layer, the overall sea ice thickness, and sets the liquid fraction of the forming platelet layer, in turn determining its volume averaged quantities. Measuring this packing efficiency amounts to measuring the porosity of the newly accreted subice platelet layer, thus far in situ measurement of this quantity has proven difficult, as the layer is remote and fragile.

Sensitivity studies were carried out wherein identical initial and boundary conditions were utilized while one of the aforementioned variables was altered from its baseline value. The results can be seen in Figure 9. It is evident that a number of variables substantially affect the evolution of the simulated sea ice, most

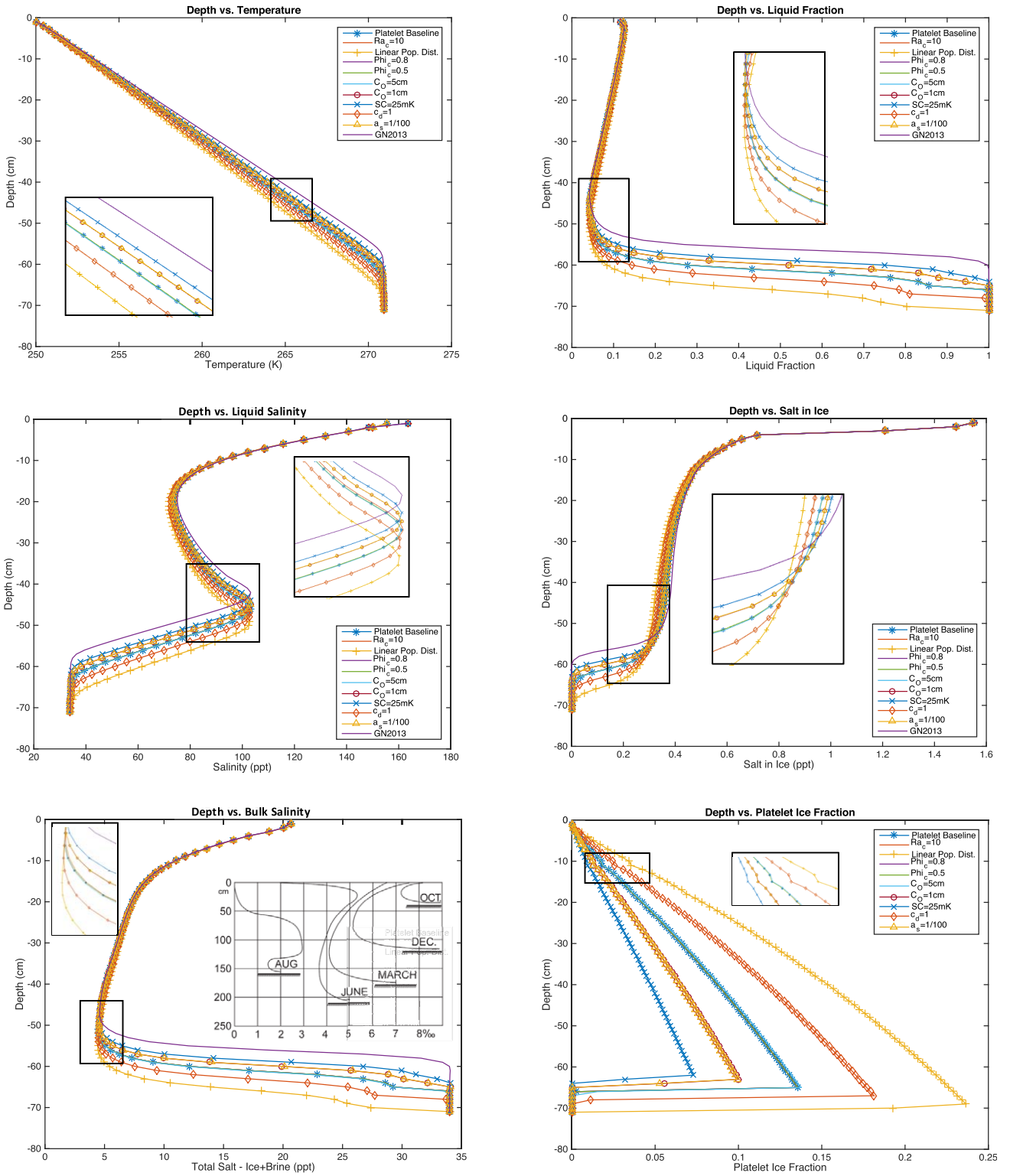

Figure 9. Plots showing the sensitivity analysis carried out by varying free parameters that dictate the dynamics of platelet ice accretion and parameterized gravity drainage (as seen in the legend: Platelet Baseline, control run; Ra_c, critical Rayleigh number; Phi_c, critical porosity for platelet accretion; c_0, platelet size cutoff for population distribution; *SC*, supercooling; c_d, drag coefficient; a_s, platelet aspect ratio). Results are from 2.0×10^6 s (~23 days) model runs. All other parameters are held constant during the simulations. Lines without symbols produce results that vary negligibly from the "Platelet Baseline" run. The inset from Malmgren (1927) shows the qualitative agreement between the numerical model and observations for total salt content in young sea ice.

notably its growth rate. Most modifications to the baseline values result in logical model outputs. Reducing the drag coefficient and considering a linear platelet size distribution, which more heavily favors larger platelets than does the baseline decreasing exponential distribution, both produce increased growth rates, while decreasing the maximum platelet size or increasing the aspect ratio of the platelets decreases growth rates. There are some properties of the platelet model that, at least on short time scales, do not affect the overall ice evolution. Both a modified critical Rayleigh number and various critical porosities determining incoming platelet packing efficiency negligibly affected the simulated ice layer. These runs were carried out for relatively short total times (2×10^6 s). Therefore, some variables that did not noticeably affect the ice during these runs could very well affect older, more slowly forming ice. Runs simulating thicker ice during the summer season explicitly showed a critical porosity cutoff where platelet ice accretion became the dominant growth mechanism, as opposed to the congelation dominated growth of young, thin ice subject to much colder atmospheric conditions. In the late season the critical porosity uniquely determined the solid fraction of the lowest layer of the forming ice (see section 4.1.1 and Figure 6).

4.3.2. Salt Distribution

Two processes that can drastically affect sea ice salinity but remain "tunable" parameters, if they are even included in models, are gravity drainage via convection and precipitated salt content. First, the convective desalination of the lower layer of forming sea ice, described in section 2.2, is the primary means of expelling salt during ice growth. The quantity of salt expelled, and thus also the final ice salinity, depends on the efficiency of the convective process. In the numerical model outlined here the primary control of this efficiency is the linear relationship assumed between the local Rayleigh number and the downward flow of brine through channels, and the associated relationship coefficient α. The default value utilized for α is based on the work of Wells et al. (2010, 2011) wherein brine channels are spaced such that potential energy is minimized and brine drainage is maximized. In reality, brine channel spacing, heterogeneous porosity, and other environmental factors could lead to less than optimal brine drainage. A number of sensitivity studies were carried out utilizing various values for α to simulate less than ideal brine drainage (Figure 10). The second factor affecting sea ice salinity is the quantity of salt precipitated out of the salt water solution contained in

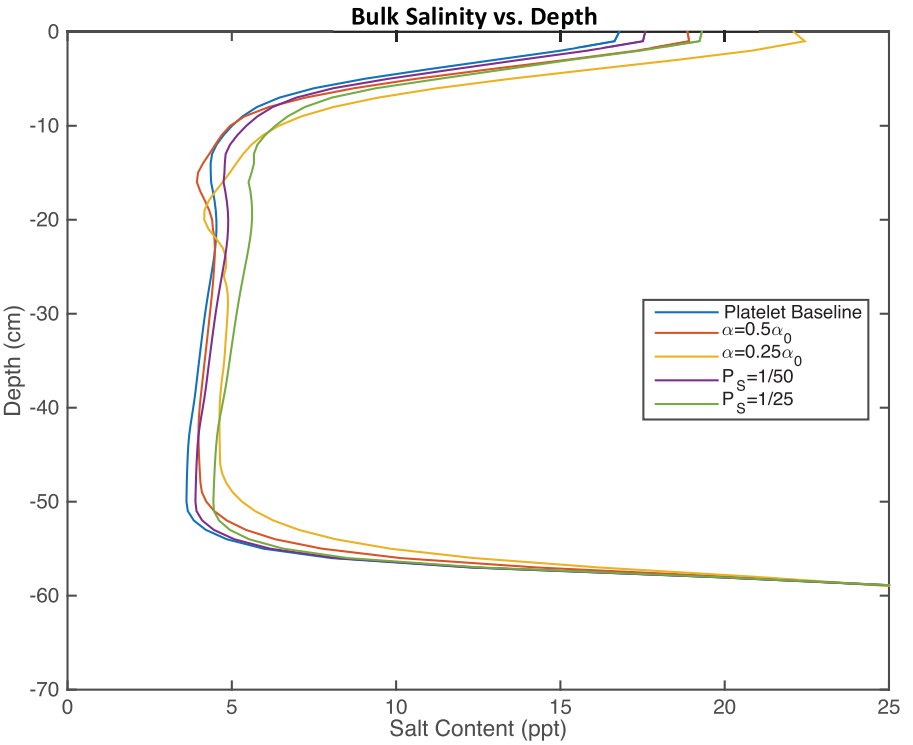

Figure 10. Plot demonstrating the sensitivity of the model to variations in parameters affecting the gravity drainage parameterization (linear relationship coefficient (α)) and partition coefficient (P_S) and the impact they have on the total salt content of growing sea ice. All runs were carried out for 2.0×10^6 s (~23 days) using the identical seasonally varying surface temperatures of Figure 2.

pockets and channels within the ice. As the temperature of seawater is depressed a variety of solid salts begin to precipitate. Due to the presence of sulfate in standard ocean water (∼8% of "sea salts") mirabilite ($H_2SO_4 \cdot 10H_2O$) begins to form at temperatures below approximately −8°C. Mirabilite is a hydrated salt and its precipitation in brine pockets and tubes of first year sea ice has been observed by Light et al. (2003). When temperatures drop below −23°C the hydrated salt hydrohalite ($NaCl \cdot 2H_2O$) begins to precipitate (Carns et al., 2015; Light et al., 2003). Precipitation of these hydrated salts has the potential to increase the overall salt content of the ice. Formation of solid salt crystals in highly concentrated, heavily cooled brine pockets and tubes prevents their expulsion back to the underlying ocean. In the current model the complex dynamics that determine precipitation rates and their dependence on temperature and salinity has been crudely represented via the partition coefficient P_S. While currently included as a tunable constant, the partition coefficient could be replaced with a complete implementation of salinity and temperature dependent salt precipitation, which will be included in future renditions of the model. Here the partition coefficient, and thus the precipitation rate, is varied to investigate its effect on the overall salt content of forming ice. The results can be seen in Figures 10 and 11.

An additional difficulty, common to many simulations of porous media flow, is determining an accurate permeability-porosity relationship. A wide range of such relationships have been proposed for sea ice (Freitag, 1999; Golden et al., 2007; Griewank & Notz, 2013; Wells et al., 2010). The default permeability-porosity

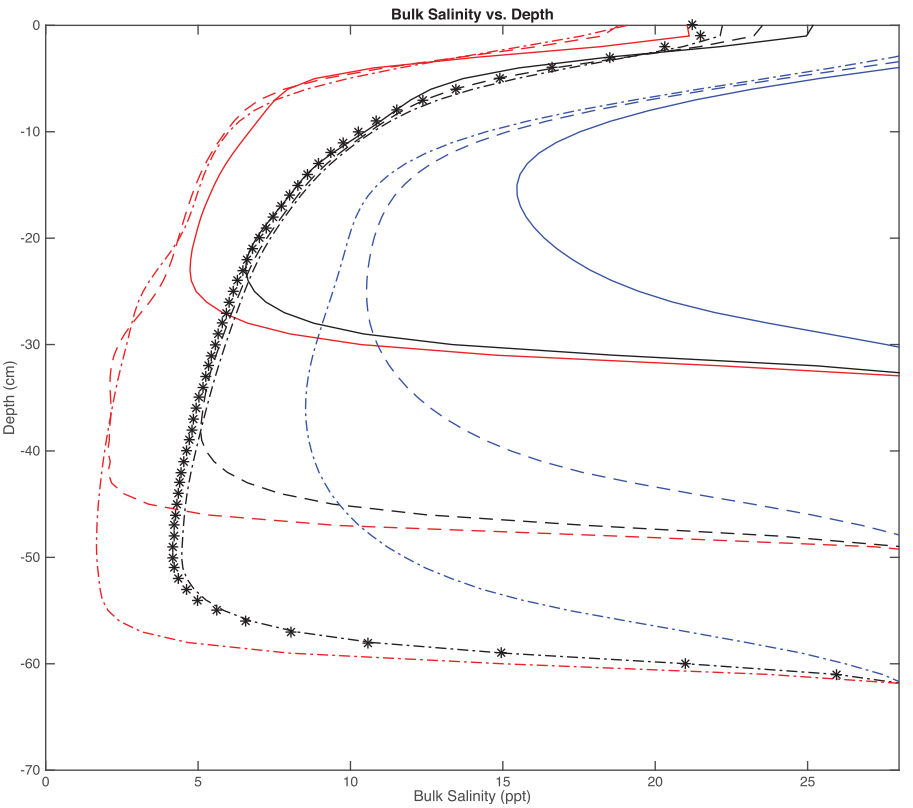

Figure 11. Plot demonstrating the effects of removing the critical porosity cutoff ($\phi < 0.05$), varying the permeability-porosity relationship ($\Pi = \Pi(\phi)$), and removing the partition coefficient (P_S) on the evolution of sea ice bulk salinity. All runs were carried out for 2.0×10^6 s (∼23 days) using a constant surface temperature of −23.15°C. Solid lines, dashed lines, and dash-dotted lines correspond to 7 days, 15 days, and 23 days after the simulation is initiated, respectively. Black lines represent model runs with $P_S = 1/100$, a porosity cutoff for $\phi < 0.05$, and the permeability-porosity relationship of GN2013 $\Pi = 10^{-17} \times \left(10^3 \times \phi\right)^{3.1}$. Red lines represent model runs with $P_S = 0$, no porosity cutoff, and the permeability-porosity relationship of GN2013. Blue lines represent model runs with $P_S = 0$, no porosity cutoff, and a modified Kozeny-Carman equation for the permeability-porosity relationship $\Pi = \left(0.5 + \frac{1}{\pi}\arctan\left[100(0.5-\phi)\right]\right) \times \left(5 \times 10^{-10}\right) \times \left(\frac{\phi^3}{(1-\phi)^2}\right)$, similar to that used by Oertling and Watts (2004). Black stars correspond to a model simulation identical to that of the black lines except $P_S = 0$ (results shown only for 23 days after initiation).

relationship implemented in the current model is the same as that used by GN2013 and is based on the empirical results of Freitag (1999). A critical porosity cutoff is implemented in the model, akin to that of Golden et al. (2007), however, others have suggested that it may be unphysical and that a finite permeability may persist even for very low porosity ice (Griewank & Notz, 2013; Petrich & Eicken, 2017). To investigate the effects of a critical porosity cutoff and various permeability-porosity relationships on the characteristics of growing sea ice, sensitivity studies were carried out. The results can be seen in Figure 11, where the default model, utilizing the permeability-porosity relationship of GN2013 with a porosity cutoff of $\phi < 0.05$ and a partition coefficient, P_S, of 1/100, is compared to simulations without porosity cutoffs or partition coefficients ($P_S = 0$), and another which utilizes an alternate permeability-porosity relationship.

The sensitivity studies clearly show that the efficiency of brine drainage and the partition coefficient influence the quantity of salt retained by the forming sea ice. The simulated ice grew to a depth of 62 cm in all cases (the bottom of the domain is not included in Figure 10 or 11 to highlight the variations in salt content within the ice). The depth-averaged salt content of the "Platelet Baseline" run (Figure 10) is 6.82 ppt, while that for $P_S = 1/25$ is 7.89 ppt. Thus, by increasing the partition coefficient by a factor of four the depth-averaged salt content increased by 1.07 ppt, equivalent to a 16% increase. For small, and likely realistic, values of the partition coefficient, assuming instead $P_S = 0$ has a negligible effect on the overall salinity of the forming ice, as can be seen in Figure 11. The depth-averaged salt content of the default model subject to a constant surface temperature (black lines in Figure 11) after 23 days is 8.73 ppt, while that of the model utilizing a modified Kozeny-Carman permeability-porosity relationship (blue lines in Figure 11) is 13.86 ppt, a 59% increase. This result suggests that, for sea ice, salt precipitation is unlikely to significantly contribute to the overall bulk salinity. Conversely, the results highlight the substantial impact permeability has on convective processes that ultimately determine the overall properties of forming sea ice and, therefore, the importance for additional constraints on permeability-porosity correlations.

5. Conclusion

Sea ice is a major component of the cryosphere, yet its chemical and thermal dynamics are typically underrepresented in large-scale Earth systems models. Complex multiphase processes that dictate the formation and evolution of sea ice have been difficult to accurately simulate, but they play a crucial role in determining energy and chemical fluxes to and from both the atmosphere and the ocean. Sea ice is relevant to the formation of water masses affecting the evolution of nearby ice shelves, exhibits unique characteristics influenced by ice shelf evolution, provides a habitat for an immense biomass crucial to the polar ocean ecosystem, and acts as an analog for ice-ocean environments elsewhere in the solar system. Numerical modeling of sea ice formation and evolution can shine light on the complex dynamics occurring in sea ice, and how these microscale physics affect the macroscale properties of the ice.

The one-dimensional, multiphase reactive transport model for sea ice, incorporating mushy layer theory, gravity drainage and an energy-conserving model of platelet ice formation and accretion, allows for a realistic treatment of sea ice near ice shelves, which can be dramatically affected by supercooled ice shelf water plumes. The inclusion of a multifaceted approach results in accurate simulation of the structural, thermal, and chemical properties observed or theorized for sea ice, as evidenced by the successful reproduction of the McMurdo Sound sea ice cores analyzed by D10. We demonstrate that minor underestimation in total salt content results from an idealized gravity drainage parameterization, which provides insight into the role that heterogeneous ice structure and nonoptimized drainage processes may play in sea ice evolution. Additionally, it was shown that platelet accretion can drastically affect the thickness (up to $\sim$15%) and properties of forming sea ice, which has implications for sea ice duration and evolution in larger scale Earth systems models.

The platelet ice accretion parameterization constitutes a novel tool for future multiphase sea ice models and offers a strategy for incorporating the ice shelf driven process of platelet ice dynamics into larger systems models. Together with the multiphase reactive transport model and gravity drainage parameterization it constitutes a numerical method with predictive abilities capable of forecasting ice structure, thickness, and characteristics in diverse ice-ocean environments. Future work will focus on utilizing the model in such a capacity.

Appendix A: Variables Used in the Text

Table A1 provides the symbol, definition, units, and value (if applicable) of all variables used throughout the text.

Table A1
Variables Used in the Text

Symbol	Definition	Units	Value
α	1-D advection coefficient		1.56×10^{-3}
$br^{\uparrow,\downarrow}$	Vertical brine transported	$m^3\ s^{-1}$	Calculated
β	Density (salinity) coefficient	kg ppt^{-1}	5.836×10^{-4}
c	Heat capacity	J kg^{-1} K^{-1}	Varies
c_d	Drag coefficient		2
c_0	Platelet size cutoff	m	0.1
dt	Time discretization	s	50
dz	Spatial discretization	m	0.01
D	Salt diffusivity	$m^2\ s^{-1}$	Calculated
H	Enthalpy	J kg^{-1}	Calculated
H_s	Enthalpy of solid cell	J kg^{-1}	Calculated
g	Acceleration due to gravity	m s^{-2}	9.8
H	Distance to interface	m	Calculated
k	Heat conductivity	W m^{-1} K^{-1}	Varies
κ	Thermal diffusivity	$m^2\ s^{-1}$	Varies
L	Latent heat of fusion (ice)	J kg^{-1}	334,774
μ	Kinematic viscosity	$m^2\ s^{-1}$	1.88×10^{-3}
ϕ	Liquid fraction		Calculated
ϕ_c	Critical porosity		0.7
P_s	Partition coefficient		1/100
ρ	Density	kg m^{-3}	Calculated
Π	Permeability	m^2	Calculated
R	Radius	m	Varies
Ra	Rayleigh number		Calculated
Ra_c	Critical Rayleigh number		1.01
S	Salinity	Ppt	Calculated
T	Temperature	K	Calculated
T_m	Melting temperature	K	Calculated
t	Time	S	
t^{adv}	Advection time scale	S	Calculated
t^{diff}	Diffusion time scale	S	Calculated
V	Platelet velocity	m s^{-1}	Calculated
w	Brine velocity	m s^{-1}	Calculated

Appendix B: An Example of Platelet Dynamics

Figure B1 illustrates platelet ice characteristics and dynamics for a hypothetical ice shelf water plume.

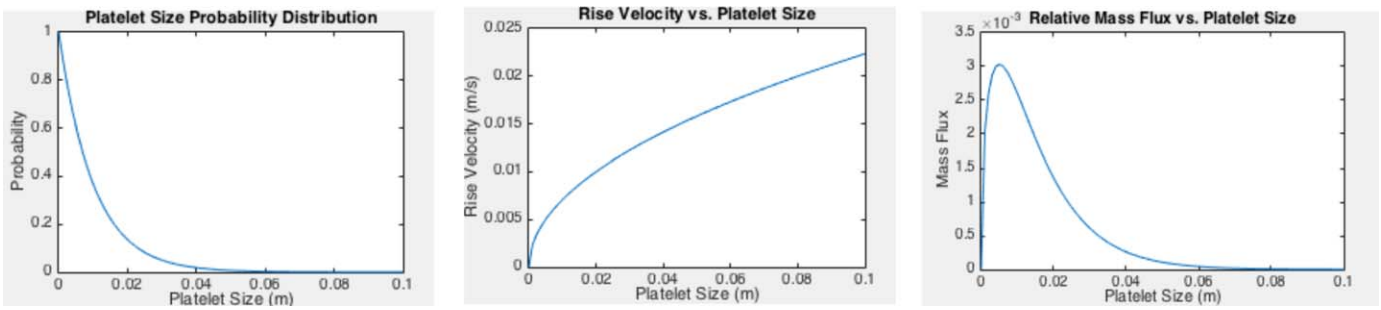

Figure B1. Plots displaying the (left) platelet size probability distribution, (middle) platelet rise velocity distribution, and (right) relative mass flux used to determine platelet ice accretion dynamics in the model. These plots were constructed using supporting information equations (S.13)–(S.16).

Acknowledgments
This study was supported by the NASA Earth and Space Science fellowship, grant NNX16AP43H and coauthor Schmidt's startup funds from the Georgia Institute of Technology. The authors thank the reviewers for their valuable comments and suggestions to improve the manuscript. Additionally, the authors thank Natalie Robinson and Mike Williams of the National Institute of Water and Atmospheric Research for helpful discussions during the course of this research. All scripts used in this publication are publicly available at schmidt.eas.gatech.edu/jacob-buffo/.

References

Aagaard, K., & Carmack, E. C. (1989). The role of sea ice and other fresh water in the Arctic circulation. *Journal of Geophysical Research: Oceans*, *94*(C10), 14485–14498. https://doi.org/10.1029/JC094iC10p14485

Arrigo, K. R., Dieckmann, G., Gosselin, M., Robinson, D. H., Fritsen, C. H., & Sullivan, C. W. (1995). High resolution study of the platelet ice ecosystem in McMurdo Sound, Antarctica: Biomass, nutrient, and production profiles within a dense microalgal bloom. *Marine Ecology Progress Series*, *127*, 255–268.

Barry, R. G., Serreze, M. C., Maslanik, J. A., & Preller, R. H. (1993). The Arctic Sea ice-climate system: Observations and modeling. *Reviews of Geophysics*, *31*(4), 397–422. https://doi.org/10.1029/93RG01998

Carns, R. C., Brandt, R. E., & Warren, S. G. (2015). Salt precipitation in sea ice and its effect on albedo, with application to snowball earth. *Journal of Geophysical Research: Oceans*, *120*, 7400–7412. https://doi.org/10.1002/2015JC011119

Cox, G. F. N., & Weeks, W. F. (1974). Salinity variations in sea ice. *Journal of Glaciology*, *13*(67), 109–120. https://doi.org/10.3189/S0022143000023418

Daly, S. F. (1984). *Frazil ice dynamics* (Rep. CRREL-MONO-84-1). Hanover, NH: Cold Regions Research and Engineering Lab.

Dayton, P. K., Robilliard, G. A., & Devries, A. L. (1969). Anchor ice formation in McMurdo Sound, Antarctica, and its biological effects. *Science*, *163*(3864), 273–274. https://doi.org/10.1126/science.163.3864.273

Dempsey, D. E. (2008). *Observation and modeling of platelet ice in McMurdo Sound, Antarctica* (MS thesis). Dunedin, New Zealand: University of Otago.

Dempsey, D. E., & Langhorne, P. J. (2012). Geometric properties of platelet ice crystals. *Cold Regions Science and Technology*, *78*, 1–13. https://doi.org/10.1016/j.coldregions.2012.03.002

Dempsey, D. E., Langhorne, P. J., Robinson, N. J., Williams, M. J. M., Haskell, T. G., & Frew, R. D. (2010). Observation and modeling of platelet ice fabric in McMurdo Sound, Antarctica. *Journal of Geophysical Research: Oceans*, *115*, C01007. https://doi.org/10.1029/2008JC005264

Eicken, H. (1992). Salinity profiles of Antarctic Sea ice: Field data and model results. *Journal of Geophysical Research: Oceans*, *97*(C10), 15545–15557. https://doi.org/10.1029/92JC01588

Eicken, H. (2003). From the microscopic, to the macroscopic, to the regional scale: Growth, microstructure and properties of sea ice. In D. N. Thomas & G. S. Dieckmann (Eds.), *Sea ice* (pp. 22–81). West Sussex, UK: Blackwell Publishing Ltd.

Eicken, H., & Lange, M. A. (1989). Development and properties of sea ice in the coastal regime of the Southeastern Weddell Sea. *Journal of Geophysical Research: Oceans*, *94*(C6), 8193–8206. https://doi.org/10.1029/JC094iC06p08193

Emms, P. W., & Fowler, A. C. (1994). Compositional convection in the solidification of binary alloys. *Journal of Fluid Mechanics*, *262*, 111–139. https://doi.org/10.1017/S0022112094000443

Feltham, D. L., Untersteiner, N., Wettlaufer, J. S., & Worster, M. G. (2006). Sea ice is a mushy layer. *Geophysical Research Letters*, *33*, L14501. https://doi.org/10.1029/2006GL026290

Freitag, J. (1999). *Hydraulic properties of Arctic sea-ice—Implications for the small scale particle transport* (Rep. Polar Res. 325). Bremerhaven, Germany: AWI, Bremerhaven (FRG).

Galton-Fenzi, B. K., Hunter, J. R., Coleman, R., Marsland, S. J., & Warner, R. C. (2012). Modeling the basal melting and marine ice accretion of the Amery Ice Shelf. *Journal of Geophysical Research: Oceans*, *117*, C09031. https://doi.org/10.1029/2012JC008214

Golden, K. M., Eicken, H., Heaton, A. L., Miner, J., Pringle, D. J., & Zhu, J. (2007). Thermal evolution of permeability and microstructure in sea ice. *Geophysical Research Letters*, *34*, L16501. https://doi.org/10.1029/2007GL030447

Goosse, H., & Fichefet, T. (1999). Importance of ice-ocean interactions for the global ocean circulation: A model study. *Journal of Geophysical Research: Oceans*, *104*(C10), 23337–23355. https://doi.org/10.1029/1999JC900215

Gough, A. J., Mahoney, A. R., Langhorne, P. J., Williams, M. J. M., Robinson, N. J., & Haskell, T. G. (2012). Signatures of supercooling: McMurdo sound platelet ice. *Journal of Glaciology*, *58*(207), 38–50. https://doi.org/10.3189/2012JoG10J218

Greeley, R., Sullivan, R., Coon, M. D., Geissler, P. E., Tufts, B. R., Head, J. W., . . . Moore, J. M. (1998). Terrestrial sea ice morphology: Considerations for Europa. *Icarus*, *135*(1), 25–40. https://doi.org/10.1006/icar.1998.5977

Griewank, P. J., & Notz, D. (2013). Insights into brine dynamics and sea ice desalination from a 1-D model study of gravity drainage. *Journal of Geophysical Research: Oceans*, *118*, 3370–3386. https://doi.org/10.1002/jgrc.20247

Griewank, P. J., & Notz, D. (2015). A 1-D modelling study of Arctic sea-ice salinity. *The Cryosphere*, *9*(1), 305–329. https://doi.org/10.5194/tc-9-305-2015

Hellmer, H. H. (2004). Impact of Antarctic ice shelf basal melting on sea ice and deep ocean properties. *Geophysical Research Letters*, *31*, L10307. https://doi.org/10.1029/2004GL019506

Holland, P. R., & Feltham, D. L. (2005). Frazil dynamics and precipitation in a water column with depth-dependent supercooling. *Journal of Fluid Mechanics*, *530*, 101–124. https://doi.org/10.1017/S002211200400285X

Hoppmann, M., Nicolaus, M., Paul, S., Hunkeler, P. A., Heinemann, G., Willmes, S., . . . Gerdes, R. (2015). Ice platelets below Weddell Sea landfast sea ice. *Annals of Glaciology*, *56*(69), 175–190. https://doi.org/10.3189/2015AoG69A678

Huber, C., Parmigiani, A., Chopard, B., Manga, M., & Bachmann, O. (2008). Lattice Boltzmann model for melting with natural convection. *International Journal of Heat and Fluid Flow*, *29*(5), 1469–1480. https://doi.org/10.1016/j.ijheatfluidflow.2008.05.002

Hughes, K. G., Langhorne, P. J., Leonard, G. H., & Stevens, C. L. (2014). Extension of an ice shelf water plume model beneath sea ice with application in McMurdo Sound, Antarctica. *Journal of Geophysical Research: Oceans*, *119*, 8662–8687. https://doi.org/10.1002/2013JC009411

Hunke, E. C., Notz, D., Turner, A. K., & Vancoppenolle, M. (2011). The multiphase physics of sea ice: A review for model developers. *The Cryosphere*, *5*(4), 989–1009. https://doi.org/10.5194/tc-5-989-2011

Hunkeler, P. A., Hoppmann, M., Hendricks, S., Kalscheuer, T., & Gerdes, R. (2016). A glimpse beneath Antarctic sea ice: Platelet layer volume from multifrequency electromagnetic induction sounding. *Geophysical Research Letters*, *43*, 222–231. https://doi.org/10.1002/2015GL065074

Huppert, H. E., & Worster, M. G. (1985). Dynamic solidification of a binary melt. *Nature*, *314*(6013), 703–707. https://doi.org/10.1038/314703a0

Jeffries, M. O., & Weeks, W. F. (1993). Structural characteristics and development of sea ice in the western Ross Sea. *Antarctic Science*, *5*(1), 63–75. https://doi.org/10.1017/S0954102093000094

Jenkins, A., & Bombosch, A. (1995). Modeling the effects of frazil ice crystals on the dynamics and thermodynamics of ice shelf water plumes. *Journal of Geophysical Research: Oceans*, *100*(C4), 6967–6981. https://doi.org/10.1029/94JC03227

Joughin, I., & Alley, R. B. (2011). Stability of the West Antarctic ice sheet in a warming world. *Nature Geoscience*, *4*(8), 506–513. https://doi.org/10.1038/ngeo1194

Kawano, Y., & Ohashi, T. (2008). Effect of salinity diffusion and heat flux on the growth of sea ice microstructure. In *23rd Northern international symposium* (pp. 1–6). Hokkaido, Japan: The Okhotsk Sea & Cold Ocean Research Association.
Khazendar, A., & Jenkins, A. (2003). A model of marine ice formation within Antarctic ice shelf rifts. *Journal of Geophysical Research: Oceans*, *108*(C7), 3235. https://doi.org/10.1029/2002JC001673
Leonard, G. H., Purdie, C. R., Langhorne, P. J., Haskell, T. G., Williams, M. J. M., & Frew, R. D. (2006). Observations of platelet ice growth and oceanographic conditions during the winter of 2003 in McMurdo Sound, Antarctica. *Journal of Geophysical Research: Oceans*, *111*, C04012. https://doi.org/10.1029/2005JC002952
Light, B., Maykut, G. A., & Grenfell, T. C. (2003). Effects of temperature on the microstructure of first-year Arctic sea ice. *Journal of Geophysical Research: Oceans*, *108*(C2), 3051. https://doi.org/10.1029/2001JC000887
Loose, B., Miller, L., Elliot, S., & Papakyriakou, T. (2011). Sea ice biogeochemistry and material transport across the frozen interface. *Oceanography*, *24*(3), 202–218. https://doi.org/10.5670/oceanog.2011.72
Malmgren, F. (1927). On the properties of sea ice. In *Norwegian north polar expedition with the 'maud', 1918–1925: Scientific results* (Vol. 1, No. 5). Bergen, Norway: Geofysisk Institutt.
Martin, S. (1981). Frazil ice in rivers and oceans. *Annual Review of Fluid Mechanics*, *13*(1), 379–397. https://doi.org/10.1146/annurev.fl.13.010181.002115
McFarlane, V., Loewen, M., & Hicks, F. (2014). Laboratory measurements of the rise velocity of frazil ice particles. *Cold Regions Science and Technology*, *106*, 120–130. https://doi.org/10.1016/j.coldregions.2014.06.009
McGuinness, M. J., Williams, M. J. M., Langhorne, P. J., Purdie, C., & Crook, J. (2009). Frazil deposition under growing sea ice. *Journal of Geophysical Research: Oceans*, *114*, C07014. https://doi.org/10.1029/2007JC004414
Meredith, M. P., & Brandon, M. A. (2017). Oceanography and sea ice in the Southern Ocean. In D. N. Thomas (Ed.), *Sea ice* (3rd ed., pp. 216–238). West Sussex, UK: John Wiley.
Notz, D. (2012). Challenges in simulating sea ice in Earth system models. *Wiley Interdisciplinary Reviews: Climate Change*, *3*(6), 509–526. https://doi.org/10.1002/wcc.189
Notz, D., & Bitz, C. M. (2017). Sea ice in Earth system models. In D. N. Thomas (Ed.), *Sea ice* (3rd ed., pp. 304–325). West Sussex, UK: John Wiley.
Notz, D., & Worster, M. G. (2009). Desalination processes of sea ice revisited. *Journal of Geophysical Research: Oceans*, *114*, C05006. https://doi.org/10.1029/2008JC004885
Oertling, A. B., & Watts, R. G. (2004). Growth of and brine drainage from NaCl-H_2O freezing: A simulation of young sea ice. *Journal of Geophysical Research: Oceans*, *109*, C04013. https://doi.org/10.1029/2001JC001109
Ohashi, T., & Kawano, Y. (2007). *Numerical simulation of salinity diffusion and growth instability in the microstructure evolution of sea ice*. Paper presented at Proceedings of the 22nd International Symposium on Okhotsk Sea and Sea Ice (pp. 11–16), Mombetsu, Japan.
Ohashi, T., Sasaki, M., & Yoshimura, K. (2004). *A numerical simulation of the development of ice-microstructures*. Paper presented at Proceedings of the 19th International Symposium on Okhotsk Sea and Sea Ice (pp. 180–185), Mombetsu, Hokkaido, Japan.
Perovich, D. K., Elder, B. C., & Richter-Menge, J. A. (1997). Observations of the annual cycle of sea ice temperature and mass balance. *Geophysical Research Letters*, *24*(5), 555–558. https://doi.org/10.1029/97GL00185
Petrich, C., & Eicken, H. (2017). Overview of sea ice growth and properties. In D. N. Thomas (Ed.), *Sea ice* (3rd ed., pp. 1–41). West Sussex, UK: John Wiley.
Rees Jones, D. W., & Worster, M. G. (2014). A physically based parameterization of gravity drainage for sea-ice modeling. *Journal of Geophysical Research: Oceans*, *119*, 5599–5621. https://doi.org/10.1002/2013JC009296
Robinson, N. J., Williams, M. J. M., Stevens, C. L., Langhorne, P. J., & Haskell, T. G. (2014). Evolution of a supercooled ice shelf water plume with an actively growing subice platelet matrix. *Journal of Geophysical Research: Oceans*, *119*, 3425–3446. https://doi.org/10.1002/2013JC009399
Schwerdtfecer, P. (1963). The thermal properties of sea ice. *Journal of Glaciology*, *4*(36), 789–807. https://doi.org/10.3189/S0022143000028379
Smedsrud, L. H., & Jenkins, A. (2004). Frazil ice formation in an ice shelf water plume. *Journal of Geophysical Research: Oceans*, *109*, C03025. https://doi.org/10.1029/2003JC001851
Smith, I. J., Langhorne, P. J., Haskell, T. G., Trodahl, H. J., Frew, R., & Vennell, M. R. (2001). Platelet ice and the land-fast sea ice of McMurdo Sound, Antarctica. *Annals of Glaciology*, *33*(1), 21–27. https://doi.org/10.3189/172756401781818365
Soderlund, K. M., Schmidt, B. E., Wicht, J., & Blankenship, D. D. (2013). Ocean-driven heating of Europa's icy shell at low latitudes. *Nature Geoscience*, *7*(1), 16–19. https://doi.org/10.1038/ngeo2021
Svensson, U., & Omstedt, A. (1994). Simulation of supercooling and size distribution in frazil ice dynamics. *Cold Regions Science and Technology*, *22*(3), 221–233. https://doi.org/10.1016/0165-232X(94)90001-9
Thomas, D. N. (2017). *Sea ice* (3rd ed.). West Sussex, UK: John Wiley.
Thomas, D. N., & Dieckmann, G. S. (2009). *Sea ice* (2nd ed.). West Sussex, UK: John Wiley.
Turner, A. K., & Hunke, E. C. (2015). Impacts of a mushy-layer thermodynamic approach in global sea-ice simulations using the CICE Sea-ice Model. *Journal of Geophysical Research: Oceans*, *120*, 1253–1275. https://doi.org/10.1002/2014JC010358
Turner, A. K., Hunke, E. C., & Bitz, C. M. (2013). Two modes of sea-ice gravity drainage: A parameterization for large-scale modeling. *Journal of Geophysical Research: Oceans*, *118*, 2279–2294. https://doi.org/10.1002/jgrc.20171
Vancoppenolle, M., Bitz, C. M., & Fichefet, T. (2007). Summer landfast sea ice desalination at point barrow, Alaska: Modeling and observations. *Journal of Geophysical Research: Oceans*, *112*, C04022. https://doi.org/10.1029/2006JC003493
Vancoppenolle, M., Meiners, K. M., Michel, C., Bopp, L., Brabant, F., Carnat, G., . . . Van Der Merwe, P. (2013). Role of sea ice in global biogeochemical cycles: Emerging views and challenges. *Quaternary Science Reviews*, *79*, 207–230. https://doi.org/10.1016/j.quascirev.2013.04.011
Wells, A. J., Wettlaufer, J. S., & Orszag, S. A. (2010). Maximal potential energy transport: A variational principle for solidification problems. *Physical Review Letters*, *105*(25), https://doi.org/10.1103/PhysRevLett.105.254502
Wells, A. J., Wettlaufer, J. S., & Orszag, S. A. (2011). Brine fluxes from growing sea ice. *Geophysical Research Letters*, *38*, L04501. https://doi.org/10.1029/2010GL046288
Wettlaufer, J. S. (2009). Sea ice and astrobiology. In D. N. Thomas & G. S. Dieckmann (Eds.), *Sea ice* (2nd ed., pp. 579–594). West Sussex, UK: John Wiley.
Wettlaufer, J. S., Worster, M. G., & Huppert, H. E. (1997). Natural convection during solidification of an alloy from above with application to the evolution of sea ice. *Journal of Fluid Mechanics*, *344*, 291–316. https://doi.org/10.1017/S0022112097006022

Wongpan, P., Langhorne, P. J., Dempsey, D. E., Hahn-Woernle, L., & Sun, Z. (2015). Simulation of the crystal growth of platelet sea ice with diffusive heat and mass transfer. *Annals of Glaciology*, *56*(69), 127–136. https://doi.org/10.3189/2015AoG69A777

Worster, M. G. (1991). Natural convection in a mushy layer. *Journal of Fluid Mechanics*, *224*, 335–359. https://doi.org/10.1017/S0022112091001787

Worster, M. G. (1997). Convection in mushy layers. *Annual Review of Fluid Mechanics*, *29*(1), 91–122. https://doi.org/10.1146/annurev.fluid.29.1.91

Worster, M. G., Huppert, H. E., & Sparks, R. S. J. (1990). Convection and crystallization in magma cooled from above. *Earth and Planetary Science Letters*, *101*(1), 78–89. https://doi.org/10.1016/0012-821X(90)90126-I

Worster, M. G., & Rees Jones, D. W. (2015). Sea-ice thermodynamics and brine drainage. *Philosophical Transactions of the Royal Society A*, *373*(2045), 20140166. https://doi.org/10.1098/rsta.2014.0166